

**TAMPA BAY ENVIRONMENTAL RESTORATION FUND
PHASE 3/ QUARTER 5/ FINAL REPORT**

PROJECT TITLE: Seeding Potential of *Pyrodinium* Cysts in Old Tampa Bay

Progress Report for the period: September 1 – December 31, 2016

Date Submitted: January 3, 2017

Contact (Name, email): Cary Lopez, cary.lopez@myfwc.com

A. What work was accomplished for this phase (1-2 paragraphs)?

We completed an additional coring trip in Old Tampa Bay on September 7, 2016. These cores were in addition to what was originally proposed.

We also completed analyses and synthesized results from the entire project. Those results are presented in the attached final report.

B. What problems (or sources of error), if any, were encountered?

We used a different methodology for retrieving cores during the September 7, 2016 coring trip to avoid diver exposure to partially treated sewage release in Tampa Bay that occurred following Hurricane Hermine (the release was ongoing at the time of sampling). Cores were visually inspected and only cores with an undisturbed sediment-water interface were kept.

C. If a problem was encountered, what action was taken to correct it?

See above, section B.

D. Is the project work on schedule?

Yes, the project work is complete.

E. If the project is not on schedule, what action is proposed to get it back on schedule?

N/A

F. What percentage of the project work has been completed to date?

100% of the proposed work is complete. We have completed all of the sampling trips and associated sample analysis. A synthesis of all results are presented in the attached final report.

G. What work is projected for the new quarter activity?

N/A

H. What deliverables/measurable benefits have been completed to date?

Phase 1 and 2 deliverables were completed and described in the Phase 1 and Phase 2 reports. Phase 3 deliverables are presented in the attached final report.

Phase 3 deliverables:

- Estimates of seeding potential (see Section 3.3 and Table 1 of final report)
- Recommendations for cyst surveys (see Section 3.4 of final report)
- Final report summarizing findings (see attached report)

TAMPA BAY ENVIRONMENTAL RESTORATION FUND

PROJECT TITLE: Seeding Potential of *Pyrodinium* Cysts in Old Tampa Bay

FINAL REPORT

Date Submitted: January 3, 2017

Primary contact:

Cary Lopez, Florida Fish and Wildlife Conservation Commission, Cary.Lopez@MyFWC.com, 727-502-4710, fax: 727- 550-4222

Project partners (co-PIs):

Christopher G. Smith (United States Geological Survey)

David J. Karlen (Environmental Protection Commission of Hillsborough County)

Alina Corcoran (Sapphire Energy, formerly Florida Fish and Wildlife Conservation Commission)

1.0 Introduction:

Local managers have restored habitats and substantially improved water quality in Tampa Bay, Florida, USA, over the last several decades. However, the recovery of Old Tampa Bay (OTB, Figure 1), the northern segment, has lagged behind other Bay segments, in part due to recurring summer blooms of the toxic dinoflagellate *Pyrodinium bahamense*. Monitoring programs have recorded bloom levels (> 5000 cells L^{-1}) of *P. bahamense* in 14 of the last 17 years (EPCHC, FWC) — with blooms now persisting, on average, 4.5 months during the summer (FWC). High biomass blooms can have cascading effects of low light penetration, degraded water quality, low dissolved oxygen, and fish kills. In addition, this alga produces saxitoxins, neurotoxins that can accumulate in filter-feeding shellfish, leading to paralytic shellfish poisoning (PSP) in humans if contaminated shellfish are consumed (Rein and Borrone 1999).

Globally, *P. bahamense* has caused more PSP-related illnesses and fatalities than any other saxitoxin-producing dinoflagellate (Azanza and Taylor 2001). In Florida, FWC permanently banned puffer fish harvesting in the Indian River Lagoon in 2002 due to accumulation of saxitoxins in puffer fish and associated cases of saxitoxin puffer fish poisoning in humans (Landsberg et al. 2006). The Florida Department of Agriculture and Consumer Services (FDACS) has also instituted extensive shellfish harvesting area closures in the Indian River Lagoon via a PSP contingency plan (FDACS, 2014). In Tampa Bay, the plan has been intermittently activated (i.e., water and shellfish meats tested), but no closures have occurred, largely because designated shellfish harvesting areas are located outside of OTB where blooms typically occur.

Pyrodinium bahamense has been documented in Tampa Bay since the 1960's, but only since 2000 has it become problematic for ecosystem health with recurring, persistent blooms. The recent shift may be attributed to the establishment and potential expansion of the *P. bahamense* seed beds (Karlen and Campbell 2012). As part of its life cycle and like many dinoflagellates, *P. bahamense* produces resting cysts, often during bloom decline, which allows the population to

remain dormant (unable to germinate) during conditions unfavorable for vegetative cell growth. The immobile, dormant cysts settle to the seafloor, creating a seed bank to initiate future blooms. Germination later occurs only after dormancy is alleviated and external (e.g., light, temperature, oxygen) factors initiate excystment (Figure 2). This strategy is comparable to that of some higher plants, in which seed production and dormancy at the end of the growing season ensure plant survival and continuation of species proliferation the following year (Geneve 2003, Finch-Savage and Leubner-Metzger 2006, Baskin and Baskin 2014).

The flux of germinated cysts from seafloor seed banks (“cyst beds”) is considered a primary driver of bloom initiation in many cyst-forming dinoflagellates (Smayda and Reynolds 2001, McGillicuddy et al. 2005). Indeed, evidence from field sampling in OTB suggests *P. bahamense* blooms initiate in areas with high abundance of cysts in the sediment (Karlen and Miller 2011, Karlen and Campbell 2012, C. Lopez unpublished data). Measures of cysts abundance in the sediment can be important to define initial location and magnitude of blooms (Stock et al. 2005), whereas the timing of dormancy release (i.e., when cysts can germinate given favorable conditions) each year is likely a primary predictor of when the bloom will initiate (Matrai et al. 2005). Therefore, understanding abundance, viability, dormancy status, and germination potential of the cyst population can provide metrics for model simulations and improve predictions of bloom initiation.

To this end, we aimed to characterize seeding potential of cyst beds in OTB. The **specific project objectives** were to:

1. quantify the vertical distribution of resting cyst abundance and viability at three sites where blooms occur in Old Tampa Bay;
2. characterize sediment mobility at the three sites using radioisotopes;
3. develop estimates of seeding potential of cyst beds based on the abundance and vertical distribution of viable cysts and estimates of sediment mobility; and
4. compare sediment sampling methods to identify the most efficient and effective method for assessing seeding potential for seasonal predictions.

We quantified cyst germination potential and sediment mobility in the upper five centimeters of sediment in environments of varying physical energy, with the premise that buried cysts may have high germination potential and serve as an important seeding source, especially in areas of increased sediment mobility. We also characterize patterns in dormancy, which complements ongoing work to describe external controls and timing of dormancy induction and release in *P. bahamense* cysts (Lopez in prep). The ultimate goal of this and future work is to develop simple indices that can be integrated into existing modeling efforts for improving predictions of bloom initiation. The work contributes to the *Charting the Course* priority to recover additional acres of seagrass by addressing the water quality problem of *P. bahamense* blooms in Old Tampa Bay.

2.0 Approach and Methods

2.1 Sediment Collection

Three sites were surveyed: TB01 (located in Safety Harbor and the most physically protected site), TB02 (south of Safety Harbor and north of Courtney Campbell Causeway) and TB06 (south of the Courtney Campbell Causeway and the most exposed of the three sites). These sites are all locations where we observe high *P.bahamense* biomass each year.

On the first four sampling dates (summer 2015, fall 2015, winter 2016, and spring 2016), sediment cores were collected using a hydraulically-damped push corer (Marot et al. 2014), which yielded undisturbed 10.2-cm diameter cores, ranging in length from 9.5 to 33 centimeters. After retrieval, cores were visually inspected for an undisturbed sediment-water interface, cores with disturbed sediment surfaces were discarded and resampled. Replicate cores were collected at TB01 during all sampling trips, at TB02 in winter and spring 2016, and at TB06 in winter 2016. Cores accepted for analysis were wrapped in opaque plastic and transported upright to the laboratory where they were kept at room temperature until extrusion and sectioning within 24 hours. On the final sampling date (summer 2016), sediment was collected by subcoring 6 x 6-inch Ekman grab samples with 10.2-cm diameter polycarbonate barrels and sectioning the uppermost 5 centimeters of sediment immediately following collection. The modified core retrieval technique on this date (7 September 2016) was used in lieu of diver-assisted retrieval to avoid exposure of divers to the partially treated sewage being released into Tampa Bay following Hurricane Hermine.

All cores were sectioned at 1-cm intervals, removing the outer circumference of each core to avoid use of sediment that came in contact with the polycarbonate tube during extrusion. The remaining sediment from each 1-cm section was collected in a clear bag and homogenized. Each section from 1 to 5 cm was sub-sampled into multiple pre-weighed amber Seal-Rite® 2.0-mL polycarbonate round-bottom tubes and weighed for quantification of cyst abundance (per sediment volume and gram wet weight) and viability by FWC. The remaining sample was used for sediment characterization by USGS.

Replicate grab samples were also collected using a Young-modified Van Veen and a petite Ponar grab sampler at site TB02 during the spring 2016 sampling to compare results using the different sampling techniques. Three replicate grab samples were collected with each sampler, and the top 1-cm sediment layer was removed from each grab and homogenized in a stainless steel beaker. The homogenized sediment was split into two subsamples: one subsample was used for the dinoflagellate cyst counts and one for sediment composition analysis (% silt/clay). The subsamples for the cyst counts were placed in opaque whirl-pack sample bags and placed in a cooler at ambient temperature and stored at 15°C within 8 hours of collection, until processing for cyst counts by FWC. The subsamples for the sediment composition analysis were transferred to pre-cleaned HDPE jars and refrigerated at 4°C until laboratory processing by EPCHC.

Water quality parameters were measured at each station using a YSI Professional Plus multi-sensor meter or a YSI 6600 VT Sonde. Measurements were recorded at 1-meter water depth and at the base of the water column. Water column profiles of temperature, conductivity, and pressure were also recorded with a SonTek Castaway-CTD sensor. Site coordinates for all trips were recorded on a vessel-mounted Garmin GPSMAP 1040xs Global Positioning (GPS) receiver.

2.2. Cyst abundance and germination potential

To develop estimates of *in situ* seeding potential, cyst abundance and germination potential in the uppermost 5 cm of sediment cores were quantified. Two sub-samples from each centimeter layer of the uppermost five centimeters were placed in the dark at room temperature and were harvested within four days to quantify cysts (cysts cm⁻³ and cysts g⁻¹ wet weight) and germination (% of cysts that germinated). The remaining subsamples from these layers were stored at 15°C in dark, anoxic conditions in Food Saver® vacuum sealer bags flushed with nitrogen gas and vacuum sealed to assess changes in dormancy, germination potential, and viability after cool storage.

To harvest cysts for measures of abundance and germination, each subsample was rinsed with 0.45 µm-filtered seawater (salinity = 25) into a 100-mL beaker and sonicated (output of eight for seven minutes using a Fisher model 100 sonicator). *Pyrodinium bahamense* cysts are approximately 50 µm in diameter, so the 20 to 130-µm size fraction was collected and intact cysts in this fraction were separated from the suspension following the addition of 1.3 g mL⁻¹ sodium polytungstate and centrifugation, which concentrated the cysts at the interface of the denser liquid and seawater. The cyst layer was collected and resuspended in a known volume of filtered seawater for subsequent isolation, incubation, and assessment of dormancy. For quantification of cyst abundance, a 5 mL aliquot was stored at 4°C and cysts were counted within seven days on an Olympus CK30 inverted microscope at 200x magnification.

Using a glass capillary, cysts were isolated from the remainder within 24 hours for assessments of germination. Individual cysts were isolated into each of the inner 60 wells of a 96-well microplate (Corning™) filled with 150 µL of 0.22 µm sterile-filtered (Corning™ sterile bottle-top filters) and autoclaved Old Tampa Bay water enriched with GSe/10 nutrients (Blackburn et al. 1989). To avoid biasing results, cysts were isolated as they were encountered without assessing the status of cyst health. Each well of the microplate was immediately checked for cyst presence using an Olympus CK30 inverted microscope at 200x magnification. Wells that contained more than one cyst were not used. Microplates were sealed with Scotch® tape, placed in clear plastic bags to prevent evaporation, and incubated at 25°C on a 12:12 light:dark cycle with illumination supplied by cool fluorescent bulbs at an average irradiance of 40 µE m⁻²s⁻¹. We incubated cysts at 25°C as this temperature is representative of spring temperatures in Old Tampa Bay and is within the optimal temperature range for *P. bahamense* cyst germination based on lab studies of nondormant cysts (Lopez unpublished).

Cysts were checked for germination microscopically at 200x magnification after seven and 14 days. Day 14 was selected as the final time point based on previous observations that non-dormant *P. bahamense* cysts rarely germinate after 14 days of incubation at 25°C (Lopez unpublished). Moreover, germination after this period could be a result of dormancy release after extended exposures to experimental temperatures rather than germination of initially non-dormant cysts (Baskin and Baskin 2014). After the incubation period, cysts were categorized using microscopy as unviable (dead), living but unable to germinate (dormant), or germinated (non-dormant). Dead cysts appeared gray and degraded under light microscopy. Cysts with this appearance also exhibited an opaque green color under epifluorescent microscopy using an

Olympus IX71 microscope equipped with a longpass blue filter set — also a marker used to identify dead cysts. A subset of cysts classified as dead (n=1206) were followed for three additional months and stasis or further degradation in cyst appearance occurred. Dormant cysts, although characterized by organized cytoplasm and pigmentation after incubation, did not germinate. Non-dormant cysts germinated by day 14, as indicated by empty cysts and a “germling” (naked or underdeveloped swimming cell) beside the empty cyst or vegetative cell swimming in the well. The fraction of unviable cysts (cysts that died) varied among cyst cohorts (i.e., cysts collected on different collection dates) for unknown reasons, so we present germination percentages of cysts scaled to the number of viable cysts when comparing patterns in dormancy and germination.

As a non-dormant control for our germination experiments, we used sediment that had been collected on 30 May 2014 using a petite Ponar grab and stored under anoxic conditions in the dark at 15°C. This ensured a reliable source of mature and non-dormant cysts as a control for the germination experiments (i.e., they were able to germinate under favorable conditions); a lack of germination in non-dormant control would indicate that experimental conditions were not optimal for germination. Periodic enumeration of cyst abundance in the control samples suggested that cysts did not degrade or germinate in storage through time. Dead cysts were not distinguished in the 2014 control, so germination rates of controls are presented as a percent of total cysts.

We compared total cyst abundance among and within seasons using two-way ANOVA on raw and rank transformed data. We employed these approaches together because the assumptions of the two-way ANOVA were not met, and both approaches employed together are recommended for confidence in results (Zar 1999). Analyses were performed in SigmaPlot 12.5.

2.3. Sediment core analysis

2.3.1. Physical Sediment Properties

A subsample of each 1-cm interval was processed for basic sediment characteristics (dry bulk density, water content, and porosity) and radionuclides. Basic sediment characteristics were calculated by determining water mass lost during drying. A known volume of each wet subsample was packed into a graduated syringe with 0.5 cm³ resolution. The wet sediment was then extracted into a pre-weighed aluminum tray and the wet sediment's weight was recorded. The wet sediment and tray were placed in a drying oven for 48 hours at 60 °C. Water content (θ) was determined as the mass of water (lost when dried) relative to the initial wet sediment mass. Porosity (ϕ) was estimated with the following equation

$$\phi = \theta / [\theta + (1 - \theta) / \rho_s],$$

where ρ_s is grain density assumed to be 2.5 g cm⁻³, the average density for siliciclastic dominated sediments. Salt-mass contributions were removed based on the salinity measured at the time of sample collection.

Organic matter content was determined with a mass loss technique, referred to as loss on ignition (LOI). The dry sediment from the previous process was homogenized with a porcelain mortar and pestle. Approximately 3-5 g of the dry sediment was placed into a pre-weighed porcelain crucible. The mass of the dried sediment was recorded. The sample was then placed inside a laboratory muffle furnace with stabilizing temperature control. The furnace was heated to 110°C for a minimum of 6 hours to remove hygroscopic water absorbed onto the sediment particles. The furnace temperature was then lowered to 60 °C, at which point the sediments could be reweighed. The dried sediment was returned to the muffle furnace. The furnace was heated to 550 °C over 30 minutes and kept at 550 °C for 6 hours. The furnace temperature was then lowered to 60 °C, at which point the sediments could be reweighed. The mass lost during the 6 hour baking period relative to the 110 °C-dried mass is used as a metric of organic matter content.

2.3.2. Grain Size Analysis

Grain size analyses were completed on all sediment intervals from the surface to 10 cm depth. Grain size analyses on the sediment cores were performed using a Coulter LS200 or LS13 320 particle size analyzer, which uses laser diffraction to measure the size distribution of sediments ranging in size from clay (0.4 µm) to very coarse-grained sand (2 mm).

Prior to particle size analysis, organic material was chemically removed from the samples using 30 % hydrogen peroxide (H₂O₂). To prevent shell fragments from damaging the Coulter instrument, particles greater than 1 mm in diameter were separated from all samples prior to analysis. The samples were washed through the sieve with deionized water and a few milliliters of sodium hexametaphosphate solution to act as a deflocculant. The sediment slurry was sonicated with a wand sonicator for 1 minute before being introduced into the Coulter LS200/LS13 320 to breakdown aggregated particles. Two subsamples from each sample were processed through the instrument a minimum of three runs apiece.

The raw grain size data were then run through the free software program GRADISTAT (Blott and Pye, 2001; <http://www.kpal.co.uk/gradistat>), which calculates the mean, sorting, skewness, and kurtosis of each sample geometrically in metric units and logarithmically in phi units (Φ) (Krumbein, 1934) using the Folk and Ward (1957) method. GRADISTAT also calculates the fraction of sediment from each sample by size category (for example, clay, coarse silt, fine sand) based on a modified Wentworth (1922) size scale.

2.3.3 Gamma Spectroscopy

Dried ground sediment from 1-cm intervals of the uppermost five centimeters of each core were used for the detection of radionuclides by standard gamma-ray spectrometry (Cutshall and Larsen, 1986) at the USGS St. Petersburg radioisotope lab. The sediments (7-30 g) were sealed in airtight polypropylene containers. The sample weights and counting container geometries were matched to pre-determined calibration standards. The sealed samples sat for a minimum of 3 weeks to allow Ra-226 to come into secular equilibrium with its daughter isotopes Pb-214 and Bi-214. The sealed samples were then counted for 24-48 hours on a planar-style, low energy, high-purity germanium, gamma-ray spectrometer. The suite of naturally occurring and

anthropogenic radioisotopes measured along with their corresponding photopeak energies in kiloelectron volts (keV) are Pb-210 (46.5 keV), Th-234 (63.3 keV), Pb-214 (295.7 and 352.5 keV; proxies for Ra-226), Be-7 (477.6 keV), Bi-214 (609.3 keV; proxy for Ra-226), Cs-137 (661.6 keV), and K-40 (1640.8 keV). Sample count rates were corrected for detector efficiency determined with IAEA RGU-1 reference material, standard photopeak intensity, and self-absorption using a U-238 sealed source (Cutshall et al., 1983).

2.4. Estimates of cyst bed seeding potential

We calculated cyst bed seeding potential (cells L⁻¹) as a function of the abundance of cysts in the sediment (cysts cm⁻³, Pb_c), the depth of sediment seeding (z_s), cyst germination potential (% germination, G), and the depth (h) of the water column (we used 4 m, the average depth of Tampa Bay, for our calculations).

$$\text{seeding potential} = \frac{Pb_c * z_s * G}{h}$$

2.5. Comparison of sampling methods

For the sampling methods comparison, the percent silt/clay in push core samples was measured as described above. The percent silt/clay in the samples collected via sediment grab sampler was measured following U.S. Environmental Protection Agency Environmental Monitoring and Assessment Program – Estuaries (EMAP-E) protocols (USEPA 1995). Approximately 20-25 grams of wet weight sediment was placed in a beaker and mixed with 20 mL of sodium hexametaphosphate (5g/l solution) and 30 mL of deionized water. The sample was stirred for 1-5 minutes then wet sieved with deionized water through a 63 μm sieve to separate the sand and silt-clay fractions. The sand fraction (> 63 μm) was transferred to a pre-weighed beaker, dried at 100° C for 24 hours and weighed after cooling to room temperature in a dessicator. The sample was dried at 100°C for an additional 24 hours and reweighed as a QA check. The final weight of the sand fraction was calculated as:

$$\text{Sand wt.} = \text{Gross wt. (sample + beaker)} - \text{beaker wt.}$$

The <63 μm filtrate fraction was transferred to a 1000 mL graduated cylinder and the volume was raised to the next 50 mL mark with deionized water. The filtrate was homogenized and a 40 mL aliquot was removed with a volumetric pipette and transferred to a pre-weighed beaker, dried at 100°C for 48 hours and weighed after cooling to room temperature in a dessicator. The sample was dried at 100°C for an additional 24 hours and reweighed for quality assurance. The final weight of the silt-clay fraction was calculated as:

$$\text{Silt-clay wt.} = [(\text{Gross wt.} - \text{beaker wt.}) \times [(\text{total volume in cylinder}) / (40\text{mL})]] - \text{dispersant weight}$$

The final percent silt-clay was calculated as:

$$\% \text{ silt-clay} = [(\text{silt-clay wt.}) / (\text{sand wt.} + \text{silt-clay wt.})] \times 100$$

A one-way ANOVA and post-hoc Holm-Sidak pairwise comparison test was used to test for significant differences between the different sampling gear using SigmaPlot 13.

3.0. Results and Discussion

3.1. Cyst abundance and viability

3.1.1. Cyst abundance

Cyst abundance was high (>1000 cysts g^{-1}) and generally uniform with depth in the uppermost five centimeters of each core (Figure 3). TB01, in Safety Harbor, exhibited slight vertical structure in the summer and fall when cyst abundance varied two fold within the core—reaching as high ~ 5000 cysts g^{-1} in the surface sediments in summer and in the 3 to 5 cm layers in fall. A two-way ANOVA on rank transformed data showed an interactive effect of season and station on variance of cyst abundance ($F(6,168) = 3.6, p=0.002$). Post-hoc multiple comparisons (Holm-Sidak) indicated summer abundance was higher than winter and spring abundance at TB01 and TB02, but not at TB06 (Figure 4). TB01 also tended to have higher cyst abundance than other stations, although the difference was not significant in summer.

The timeframe of the summer and fall core sampling coincided with a precipitous *P. bahamense* bloom decline in the water column, which was most notable at TB01 in early August when freshwater input reduced salinity below 10 psu (FWC, data not shown). Therefore, we can speculate that there was a high flux of cysts from the water column to the sediment in late summer into early fall, which might explain the elevated surface cyst abundance at that time, which was evident at all stations but most dramatic at TB01 (Figure 4, Figure 5).

3.1.2. Dormancy expression and release

The germination potential of cysts collected from the field varied seasonally from high dormancy (low cyst germination) in the summer and fall to minimal dormancy (peak cyst germination) in the spring. This pattern was consistent across stations and sediment depths (Figure 6). Less than 1% of cysts collected in the summer and fall of 2015 germinated upon incubation. In contrast, almost half ($49 \pm 20\%$) of viable cysts (12% of total cysts) collected in winter germinated. By spring of 2016, the majority of cysts collected from the field had high germination (with $90 \pm 10\%$ viable cysts germinating, Figure 7). We observed no germination by field cysts in September 2016, indicating cysts had returned to a dormant state. Cysts from 10 cm sediment depth—which were presumably older—exhibited similar patterns in *in situ* dormancy expression (data not shown) as the cysts collected in the uppermost five centimeters of sediment. Further, non-dormant control cysts, which had been collected in 2014, germinated consistently over the study period with no notable pattern in dormancy expression or change in germination potential (Figure 7). Combined, these results suggest that dormancy was not a function of cyst maturity or an internal clock independent of seasonal temperature cycling.

3.2. Sediment characterization

Measurements of bulk density used the entire core lengths, whereas grain size was measured for the 0-10 cm intervals, and radioisotope activity for the uppermost 5cm. For consistency with cyst and radioisotope data, all descriptions on sediment texture reference the top 5 cm. Profiles of all cores are presented in Appendix I.

3.2.1. Physical Characteristics

Sediment grain size, sorting (which is essentially a normalized variance that describes the distribution of grain size, with increasing numbers reflecting more poorly sorted sediment), % organic matter, and % mud are presented herein as measures to characterize the sediment physically (see Appendix I for all sediment profiles).

Replicate cores collected from TB01 showed excellent agreement in physical characteristics on most sampling dates. Overall, sediments at TB01 were the finest-grained sediment and the highest organic matter of the three sample locations. The sediment at TB01 were very poorly sorted, coarse silts. Mean grain size and sorting were vertically homogeneous in the upper 5 cm and relatively constant throughout the study. The mean grain size ranges for core replicates (TB01-A and TB01-B) were 19.2 – 28.0 μm and 19.5 – 36.0 μm , respectively. The mean grain size for the fall core TB01-B was qualitatively coarser than the overall mean of both core replicates; however, such small differences are unlikely to affect sediment mobility. Similarly, the fraction of mud for all TB01 cores was approximately 60% except for the fall TB01-B core, which had lower (49%) mud content. The organic matter content was slightly more variable among cores, but averaged approximately 10%. There was a slight increase in organic matter through time (approximately 2% increase from first sampling trip to last, within the detectable precision of the loss-on-ignition method).

Cores collected north of the Courtney-Campbell Causeway, at TB02, had higher temporal and horizontal (within-site) spatial variability in sediment parameters compared to other sites. While the upper 5-cm of sediment was homogeneous for each sampling trip, the sediment texture ranged among seasons from a very poorly sorted, very coarse silt to a poorly sorted, very fine sand. The mean grain size for all cores ranges from 61.0 to 113 μm and sorting from 3.28 to 4.56 μm . Mean grain size in the upper five cm of the duplicate winter TB02 cores was significantly different (ANOVA, $F(1,8) = 14.27$, $P = 0.05$), but the variability between the two winter cores was not statistically different than the temporal variability observed among cores collected in other seasons (ANOVA, $F(1,23) = 1.872$; $P = 0.184$). There was no significant difference observed between the September 2016 core duplicates ($F(1,8) = 0.038$; $P = 0.85$). While we did observe within-site spatial variability in winter, the functional sediment type—very coarse silt and very fine sand— are not geologically that different. The increase in grain size and decrease in sorting at TB02, relative to TB01, was a reflection of a decrease in the overall fine (mud) content in the sediment at this site. The average mud content for the top 5-cm ranged from 20 to 30% among the TB02 cores with no specific temporal pattern. Like cores from TB01, organic matter had a variability of around 2% for all the cores with a range of 5.0 to 7.4%. The organic matter content was positively correlated with the mud content suggesting that the bulk of the organic matter was in the finer size fraction.

Cores collected south of the Courtney-Campbell Causeway, TB06, had the coarsest sediment of all the sampled locations. The sediment sorting at site TB06 was functionally poorly to moderately sorted, fine sand. Like the other sites, the upper five cm of sediment was vertically homogeneous. The relative range in mean grain size among the cores was 20% (138 – 170 μm). Sorting in the sediment ranged from 1.74 to 2.28 μm . Mud content and organic matter were positively correlated. The mud content varied from 6.7 to 12.2 % and organic matter varied from 1.6 to 2.8 % with the highest fraction of mud observed in summer 2015 and a steady decline noted through summer 2016.

3.2.2. Radionuclides

The radionuclides beryllium-7 (^7Be), lead-210 (^{210}Pb), and radium-226 (^{226}Ra) were quantifiable in every core. These radionuclides, and their utility for measuring sediment processes, are described in Appendix I for reference. Thorium-234 was inconsistently observed and thus the results are not presented here, but are provided in Appendix I. Among all the sites, the range in ^7Be activity was 0.38 to 10.13 dpm g^{-1} . ^7Be occurred at variable depths through space and time with an overall average depth of roughly 2.3 cm (Figure 8A). The only spatially consistent pattern observed was during February 2016, when ^7Be was restricted to the surficial sediments (0-1 cm, Figure 8A). Surface activities and inventories of ^7Be were generally higher during wet season (May – October) than during the dry season (November-April) (Figure 8B).

Overall, the range in total ^{210}Pb (sediment supported and atmospherically-derived) and ^{226}Ra were 2.95 – 13.24 dpm g^{-1} and 1.27 – 3.30 dpm g^{-1} , respectively. The corresponding range in excess ^{210}Pb activity (atmospherically-derived) was 1.61 – 10.23 dpm g^{-1} . The parent-(grand) daughter isotope pair, ^{226}Ra and ^{210}Pb , did vary temporally but not with the same magnitude as ^7Be . In contrast to ^7Be , the spatial difference between upper bay and the lower bay dominated the signal in these isotopes. The highest activities of total ^{210}Pb , ^{226}Ra , and excess ^{210}Pb were observed exclusively at TB01 and their activities decreased down the bay to TB06.

3.2.3. Factors influencing radioisotope distributions in the sediment

The temporal variability of ^7Be and, to a lesser extent, excess (atmospherically-derived) ^{210}Pb in the surface samples (0-1 cm) suggest that there may be an underlying temporal driver in the accumulation of these radionuclides in the shallow sediments. Salinity and precipitation data recorded during the course of this study support Florida's monsoonal climatology (Figure 9). Beryllium-7, and to a lesser extent, excess ^{210}Pb activity increased slightly during the wetter, summer months compared to the dryer months. This pattern is exemplified when ^7Be is normalized by the observed excess ^{210}Pb activity for each surface sediment ($^7\text{Be}:^{210}\text{Pb}_{\text{ex}}$, Figure 8D). While the temporal duration of the data set was too short to quantify seasonality, the spatial consistency of observed temporal trends at all sites favor a coherent temporal process of enhanced ^7Be supply during the wet months.

We used principal component analysis (PCA) to explore relationships among radionuclide data, salinity, and sediment textural data (Figure 10). The contrast of the temporal variability of ^7Be with the spatial variability of excess ^{210}Pb was an important factor separating PC1 from PC2.

Loadings of ^{210}Pb , ^{226}Ra , and excess ^{210}Pb align nearly uniformly with PC1 (69.5% of variance explained), and the close clustering of the parent, daughter, and excess daughter isotopes suggested a similar factor influencing variance. Correlated with these were fine-grained sediment metrics, such as percent mud and organic matter content. Salinity aligns closely and positively with PC2 (22.0%) suggesting freshwater input was a major contributor to the variance defined by PC2. Both ^7Be and the ratio of ^7Be to excess ^{210}Pb are strongly negatively correlated with salinity and PC2, which supports the hypothesis that salinity (and presumably precipitation) were major contributors to ^7Be delivery to the sediment.

These PCA analyses also highlighted the contrast in the environmental residence time of ^7Be and ^{210}Pb in surficial sediments of Tampa Bay; results suggest that ^7Be (53.3 day half-life) was driven by freshwater inflows during the wet season. As ^7Be is supplied via freshwater run-off from the surrounding land and discharge from Lake Tarpon, ^7Be would be scavenged by sedimentary particles settling through the water column and delivered to the sediment. The timing of the pulse in ^7Be delivery overlapped with the *P. bahamense* bloom period and, likely, cyst production and settling to the sea-bed (section 3.1.1). The decrease of ^7Be activity in the dry months (Figure 8) suggests that the supply of ^7Be has been reduced and decay in the sediment exceeded source terms. Considering that excess ^{210}Pb (22.3 year half-life) is also produced in the atmosphere, it is expected that the maximum flux of excess ^{210}Pb would coincide with other atmospherically derived tracers like ^7Be (Baskaran and Swarzenski, 2007). When we consider the surface sediments, we find that the excess ^{210}Pb activity was relatively uniform through time at all stations. This persistent nature could reflect two possible scenarios: 1) supply of excess ^{210}Pb and ^7Be to the surficial sediments, either from the atmosphere or within the water column, were decoupled, or 2) supply of the radionuclides was proportional throughout the year, but the longer half-life of excess ^{210}Pb causes a more temporally homogeneous record. The latter is more consistent with the general understanding of geochemistry of these two particle tracers (Canuel et al. 1990; Baskaran and Swarzenski, 2007), and is also consistent with atmospheric flux data presented by Baskaran and Swarzenski (2007). They found that between July 2003 and July 2004 the atmospheric deposition of ^{210}Pb and ^7Be were highly correlated; they also argue that freshwater discharge and sediment resuspension control their distribution in the water column. Our data show that the freshwater discharge appears to be a major control on ^7Be supply and that ^7Be is not restricted solely to the surface sediments.

Spatial variability is prevalent in the data set and provides difficulty in truly quantitative application of the radionuclide data. Nevertheless, we have found semi-quantitative evidence that the temporal variability exceeds, at least at most sites, the spatial variability.

3.2.4. Vertical mobility of sediment

Evidence from ^7Be radionuclide data supports the hypothesis that there is vertical movement of sediment in the upper 5 cm, which has important implications for cyst bed dynamics. The presence of ^7Be to depths below the surface centimeter (Figure 8) suggest that (outside of coring bias) the sediments below 0-1 cm had been in contact with an atmospheric source of ^7Be between 79 days (mean life of ^7Be) and one year (~6 half-lives) prior to sampling, depending on the initial ^7Be activity. The mean depth of ^7Be penetration over the study period was 2.3 cm, with a maximum of 5 cm at TB02 during the summer and fall of 2015. The mechanism for

reworking sediment to these depths is not well constrained by the data collected, but may be related to site specific characteristics. For example, meio- to macro-fauna burrowing life habits could explain sediment reworking; bioturbation in estuarine systems, including Tampa Bay, is a well-documented process (Klerks et al. 2007). Alternatively, sediment resuspension and resettling could be important. Considering that the sites range from high clay to low clay content, the role of resuspension and settling varies considerably. The critical shear stress needed to resuspend sediments with greater than 7-8% clay (e.g., all TB01 cores) are difficult to address as cohesion is a prominent force, but for sediments with less than 7% clay (all TB02 and TB06 cores), a strong relationship exist between mean or median grain size and critical shear stress (Wiberg and Smith, 1987). Further studies are required to refine the mechanism for vertical sediment mobilization at these sites. Regardless, the vertical movement indicates that sub-surface sediment may play a role in the supply of cysts for seeding the water column—whether through their gradual introduction to the oxygenated surface sediment layers via bioturbation or through pulses injected into the water column via resuspension events.

3.3. Calculations of seeding potential

We found high cyst abundance throughout the upper five centimeters at all stations and in all seasons. However, the cysts were dormant and unable to germinate in the summer and fall (Figure 9), so the cyst beds at this time of year had little to no potential to seed the water column with vegetative cells (the bloom was also in decline during the summer 2015 sampling and was gone by the fall sampling). These findings are supported by a complementary project that has shown that summer temperatures induce dormancy in *P. bahamense* cysts, which then require extended winter temperature exposure (between 100-120 days) to break from dormancy (Lopez et al. in prep). Such a strategy may allow the algae to ‘overwinter’—in effect, synchronizing the timing of dormancy release to occur in late winter or early springtime when conditions in the water column are becoming more favorable for vegetative cell growth. Indeed, we found that by the winter 2016 sampling, cysts collected from the field were beginning to germinate and by spring 2016—the time when vegetative cells were first observed in the water column—cysts were germinating at their maximum potential (Figure 7). These results are also consistent with observance of the *P. bahamense* bloom cycle in prior years, which generally begins by mid-May and ends by late-September (Lopez et al. in prep).

Together, these findings provide promise for refining our understanding and predictions of bloom timing. Building on lessons from the field of plant ecology in which simple metrics such as chilling hours are used to predict when dormant fruit buds will bloom (Sedgley and Griffin 1989), we calculated “accumulated cooling hours” to explore its use in predicting germination timing for *P. bahamense* cysts. We used hourly water temperature data from Tampa Bay (NOAA CO-OPS buoy 872650, www.tidesandcurrents.noaa.gov), to calculate an index of accumulated hours below 25°C *in situ* for each winter in the years between 2012 and 2016, and found a significant relationship between this metric and bloom timing for these years ($y = 1.2x - 12.2$, $R^2=0.93$, $p=0.007$, Lopez unpublished). For example, for the 2016 bloom season, we found the time of year that coincided with a 100-120 day cooling window was between March 12 and April 1, 2016. Similarly, *P. bahamense* vegetative cells were first detected in the water column (through twice monthly routine sampling) on April 14, 2016 (at 667 cells L⁻¹). These preliminary analyses suggest accumulated cooling hours could be a simple index to explore for predicting the

timing of bloom initiation. More research is needed, however, to define the cooling requirements (temperature threshold and duration) for dormancy release as well as to assess its reliability and utility.

The magnitude of seeding is also an important metric needed to characterize bloom initiation. We calculated “seeding potential” as a hypothetical estimate of the magnitude of seeding. In winter and spring of 2016, we observed significant germination in field-collected cysts, so we used this discrete germination data along with cyst abundance to calculate seeding potential at these timepoints. An important unknown, however, was the depth of sediment available to seed the water column under given scenarios. The radionuclide results indicate some degree of sediment mobility in the top five centimeters, so it is possible that cysts below the surface layer may contribute to the functional seed reservoir. Therefore, we calculated cyst flux over a range of hypothetical sediment seeding depths (z_s : 1mm, 1cm, 5cm). We applied the calculation of cyst flux to a water column depth of 4 m (average depth of Tampa Bay) to calculate the hypothetical initial vegetative cell concentrations in the water column (Table 1). This exercise illustrated the potential importance of sediment seeding depth relative to the variability in germination potential and cyst abundance, with an order of magnitude difference in initial cell concentration in the water column when 1 cm of sediment seeded the water column vs. 1 mm. Other factors with clear, but undefined, importance to the translation of cell inoculation to bloom initiation are 1) the fraction of germinated cells that survive to the swimming/dividing stage and 2) the environmental conditions in the water column that promote optimal vegetative cell growth. Further, a somewhat continuous seeding of cysts in the early stages of bloom development as buried sediment becomes exposed to the oxygenated layer through bioturbation and/or resuspension is a possible scenario to be considered.

Table 1. Calculations of seeding potential as initial *P. bahamense* cell concentration in the water column.

	Mean cyst abundance (cysts cm ⁻³)	Germination potential of cysts (% of total cysts germinating)	Hypothetical sediment seeding depth (cm)	Initial cell concentration (vegetative cells L ⁻¹)
Winter	1470	0.12	0.1 cm	44
			1.0 cm	440
			5.0 cm	2205
Spring	1300	0.31	0.1 cm	101
			1.0 cm	1010
			5.0 cm	5040

3.4 Methods comparison and cyst survey recommendations

Overall, the petite Ponar had significantly higher mud (silt and clay) results compared to the Van Veen and core samples ($p < 0.001$), but there was no significant difference between the core and Van Veen results. Moreover, although mean cyst abundance was lowest in the petite Ponar samples, there was no significant difference in cyst abundance among the sampling methods (Figure 11). While we only compared gear at one station, the results suggest that for cyst surveys

in OTB, the easier and more cost effective grab sampling technique would be sufficient for capturing cyst abundance in the top several cm of sediment. Overall, the Van Veen grab sampler gave results that were most similar to the core sampler, so its use would be recommended over a petite Ponar if available and practical.

In recent years, the general pattern of *P. bahamense* blooms has been mostly predictable from year to year, but there are variations among years that present challenges for planning and allocating of management resources. For example, in 2012 and 2015, the bloom began a month earlier than usual, which resulted in a five month long bloom period. In 2012, there was also a bi-modal bloom, which suggests re-seeding of the water column or a resurgence in cell growth occurred (FWC data not shown). Understanding and being able to anticipate these differences would require cyst surveys prior to the bloom period in order to accurately characterize the flux of germinated cysts that drives the initiation. Because significant changes in cyst abundance and distribution were observed over the course of a year, we recommend late winter as the optimal time for a cyst survey to capture cyst abundance in the time period prior to bloom initiation. Finally, estimates of germination timing and the magnitude of seeding potential need to be complemented by interdisciplinary research on cell physiology and bloom ecology to effectively model and predict blooms of *P. bahamense*.

References

- Anderson, D. M., C. A. Stock, B. A. Keafer, A. Bronzino Nelson, B. Thompson, D. J. McGillicuddy, M. Keller, P. A. Matrai and J. Martin. 2005. "Alexandrium fundyense cyst dynamics in the Gulf of Maine." *Deep Sea Research Part II: Topical Studies in Oceanography* 52(19-21): 2522-2542.
- Azanza, R. V. and F. J. R. M. Taylor. 2001. "Are Pyrodinium Blooms in the Southeast Asian Region Recurring and Spreading? A View at the End of the Millennium." *AMBIO: A Journal of the Human Environment* 30(6): 356-364.
- Baskaran, M., Swarzenski, P.W. 2007. Seasonal variations on the residence times and partitioning of short-lived radionuclides (Th-234, Be-7 and Pb-210) and depositional fluxes of Be-7 and Pb-210 in Tampa Bay, Florida. *Marine Chemistry* 104, 27-42.
- Baskin, C., J. Baskin. 2014. *Seeds: Ecology, biogeography, and evolution of dormancy and germination*. Academic Press. San Diego.
- Blackburn, S.I., Hallegraeff, G.M., and Bolch, C.J. 1989. Vegetative reproduction and sexual life cycle of the toxic dinoflagellate *Gymnodinium catenatum* from Tasmania, Australia. *J. Phycol.* 25: 577-590.
- Blott, S. J., and K. Pye. 2001. Gradistat: A grain size distribution and statistics package for the analysis of unconsolidated sediments. *Earth Surface Processes and Landforms* 26: 1237-1248.
- Bolch, C.J.S. 1997. The use of sodium polytungstate for the separation and concentration of living dinoflagellate cysts from marine sediments. *Phycologia* 36(6), 472-478.
- Canuel, E.A., Martens, C.S., Benninger, L.K. 1990. Seasonal-variations in Be-7 activity in the sediments of Cape Lookout-Bight, North-Carolina. *Geochimica Et Cosmochimica Acta* 54, 237-245.
- Cutshall, N.H., Larsen, I.L., and Olsen, C.R. 1983. Direct analysis of ²¹⁰Pb in sediment samples: self-absorption corrections: *Nuclear Instruments and Methods*, v. 206, nos. 1-2, p. 309-312. [Also available at [http://dx.doi.org/10.1016/0167-5087\(83\)91273-5](http://dx.doi.org/10.1016/0167-5087(83)91273-5).]
- Cutshall, N.H., and Larsen, I.L. 1986. Calibration of a portable intrinsic Ge gamma-ray detector using point sources and testing for field applications: *Health Physics*, v. 51, no. 1, p. 53-59. [Also available at <http://dx.doi.org/10.1097/00004032-198607000-00004>.]
- FDACS, 2014. Contingency plan for the control of shellfish potentially contaminated by marine biotoxin, Tallahassee.
- Folk, R. L., and W. C. Ward. 1957. Brazos river bar: A study in the significance of grain size parameters. *Journal of Sedimentary Petrology* 27: 3 - 26.

Karlen, D., Campbell, K. 2012. The distribution of Pyrodinium bahamense cysts in Old Tampa Bay sediments, Tampa Bay Estuary Program Technical Report. Environmental Protection Commission of Hillsborough County, Tampa.

Klerks, P.L., Felder, D.L., Strasser, K., Swarzenski, P.W. 2007. Effects of ghost shrimp on zinc and cadmium in sediments from Tampa Bay, FL. Marine Chemistry 104, 17-26.

Krumbein, W.C., 1934, Size frequency distributions of sediments: Journal of Sedimentary Petrology, v. 4, no. 2, p. 65–77. [Also available at <http://dx.doi.org/10.1306/D4268EB9-2B26-11D7-8648000102C1865D>.]

Landsberg, J. H., S. Hall, J. N. Johannessen, K. D. White, S. M. Conrad, J. P. Abbott, L. J. Flewelling, R. W. Richardson, R. W. Dickey, E. L. E. Jester, S. M. Etheridge, J. R. Deeds, F. M. Van Dolah, T. A. Leighfield, Y. Zou, C. G. Beaudry, R. A. Benner, P. L. Rogers, P. S. Scott, K. Kawabata, J. L. Wolny and K. A. Steidinger. 2006. "Saxitoxin Puffer Fish Poisoning in the United States, with the First Report of Pyrodinium bahamense as the Putative Toxin Source." Environmental Health Perspectives 114(10): 1502-1507.

Lopez, C., A. Karim, A. Corcoran. (in prep). Temperature-mediated dormancy cycling in *Pyrodinium bahamense* (DINOPHYCEAE) in Tampa Bay, Florida, USA.

Marot, M.E., Adams, C.S., Richwine, K.A., Smith, C.G., Osterman, L.E., Bernier, J.C. 2014. Temporal changes in lithology and radiochemistry from the back-barrier environments along the Chandeleur Islands, Louisiana—March 2012–July 2013: U.S. Geological Survey Open-File Report 2014-1079, 1 DVD, <http://dx.doi.org/10.3133/ofr20141079>.

McGillicuddy, D.J., Anderson, D.M., Lynch, D.R., Townsend, D.W. 2005. Mechanisms regulating large-scale seasonal fluctuations in Alexandrium fundyense populations in the Gulf of Maine: Results from a physical biological model. Deep-Sea Research Part II 52(19-21), 2698-2714.

Meyers, S.D., Luther, M.E., Wilson, M., Havens, H., Linville, A., Sopkin, K. 2007. A Numerical Simulation of Residual Circulation in Tampa Bay. Part I: Low-frequency Temporal Variations. Estuaries and Coasts 30(4): 679-697

Matrai, P., B. Thompson and M. Keller. 2005. "Circannual excystment of resting cysts of Alexandrium spp. from eastern Gulf of Maine populations." Deep Sea Research Part II: Topical Studies in Oceanography 52(19-21): 2560-2568.

Rein, K. S. and J. Borrone. 1999. "Polyketides from dinoflagellates: origins, pharmacology and biosynthesis." Comparative Biochemistry and Physiology B-Biochemistry & Molecular Biology 124(2): 117-131.

Sedgley, M. and A.R. Griffin. 1989. Sexual Reproduction of Tree Crops. Academic Press. 378 pp.

Smayda, T.J., Reynolds, C.S. 2001. Community Assembly in Marine Phytoplankton: Application of Recent Models to Harmful Dinoflagellate Blooms. *Journal of Plankton Research* 23(5), 447-461.

Stock, C.A., McGillicuddy, D.J., Solow, A.R., Anderson, D.M. 2005. Evaluating hypotheses for the initiation and development of *Alexandrium fundyense* blooms in the western Gulf of Maine using a coupled physical-biological model. *Deep-Sea Research II*, 52(19-21), 2715-2744.

Wentworth, C.K. 1922. A scale of grade and class terms for clastic sediments: *Journal of Geology*, v. 30, no. 5, p. 377–392. [Also available at <http://dx.doi.org/10.1086/622910>.]

Wiberg, P.L., Smith, J.D. 1987. Calculations of the critical shear stress for motion of uniform and heterogeneous sediments. *Water Resources Research* 23, 1471-1480.

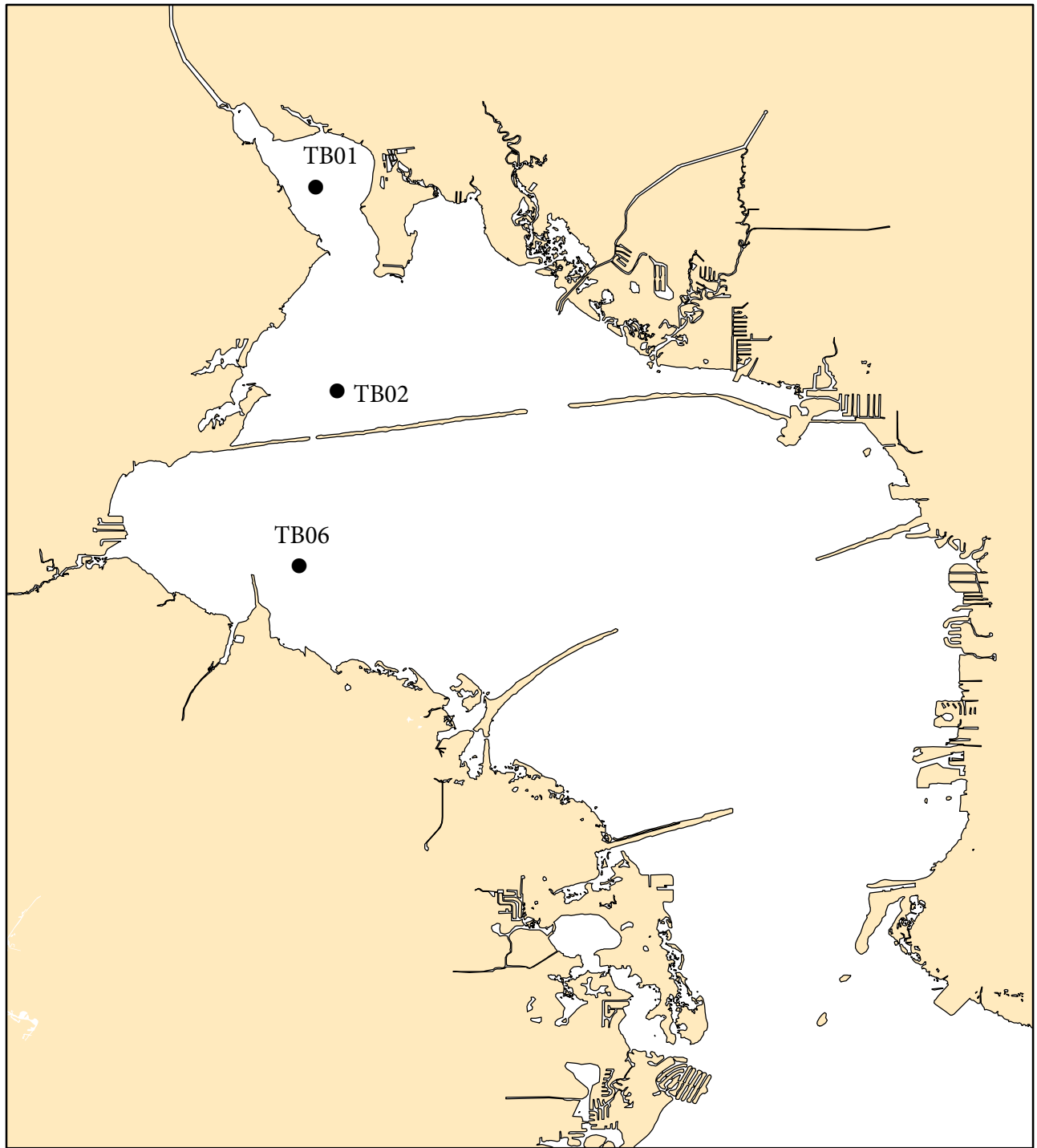


Figure 1. Map of Old Tampa Bay and coring sites, TB01, TB02, and TB06

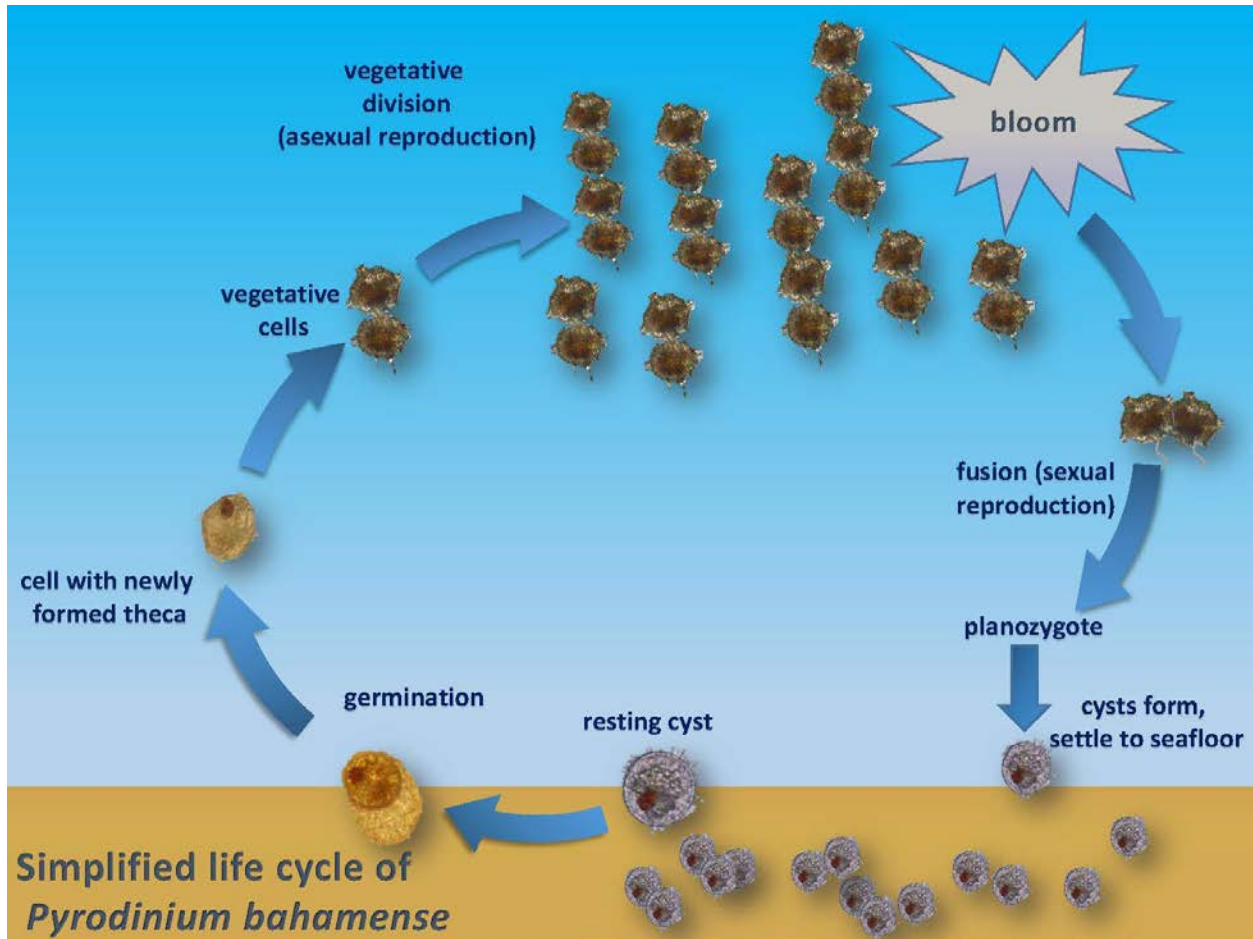


Figure 2. Simplified life cycle of the dinoflagellate *Pyrodinium bahamense*, showing germination and transformation from a resting cyst to a vegetative, dividing cell and back to the sexual resting stage that settles to the seafloor.

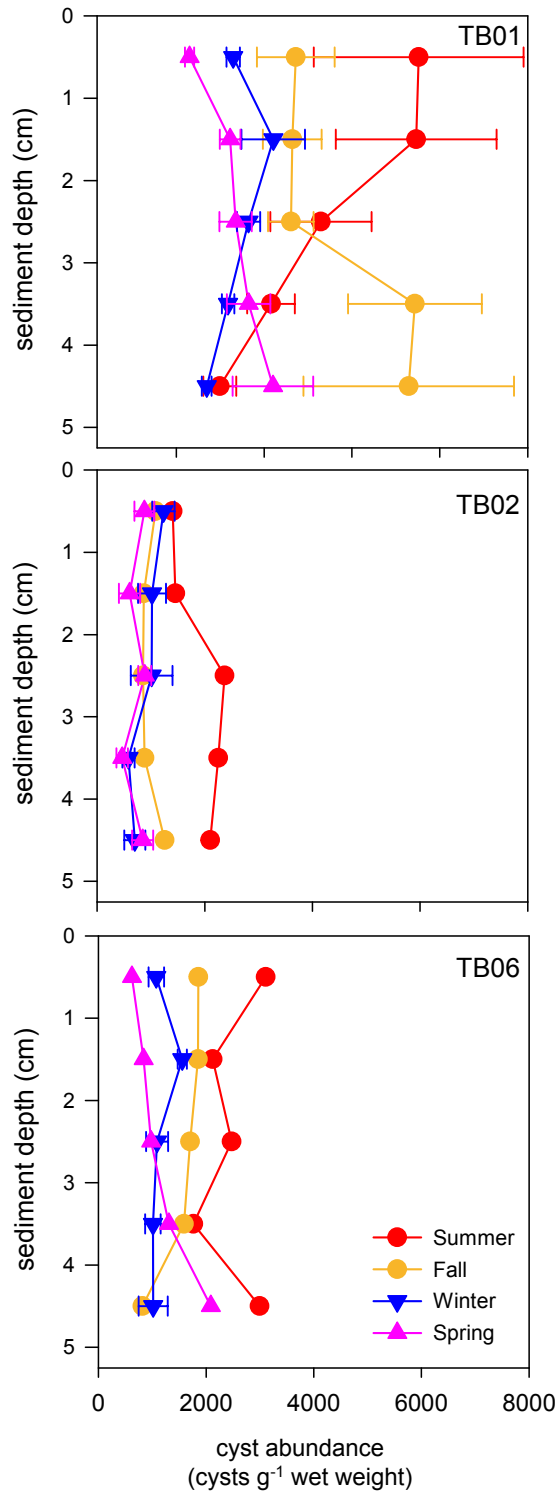


Figure 3. Vertical profiles of cyst abundance (mean \pm standard error of core replicates) in the upper five centimeters of sediment for TB01 (upper panel), TB02 (middle panel), and TB06 (lower panel).

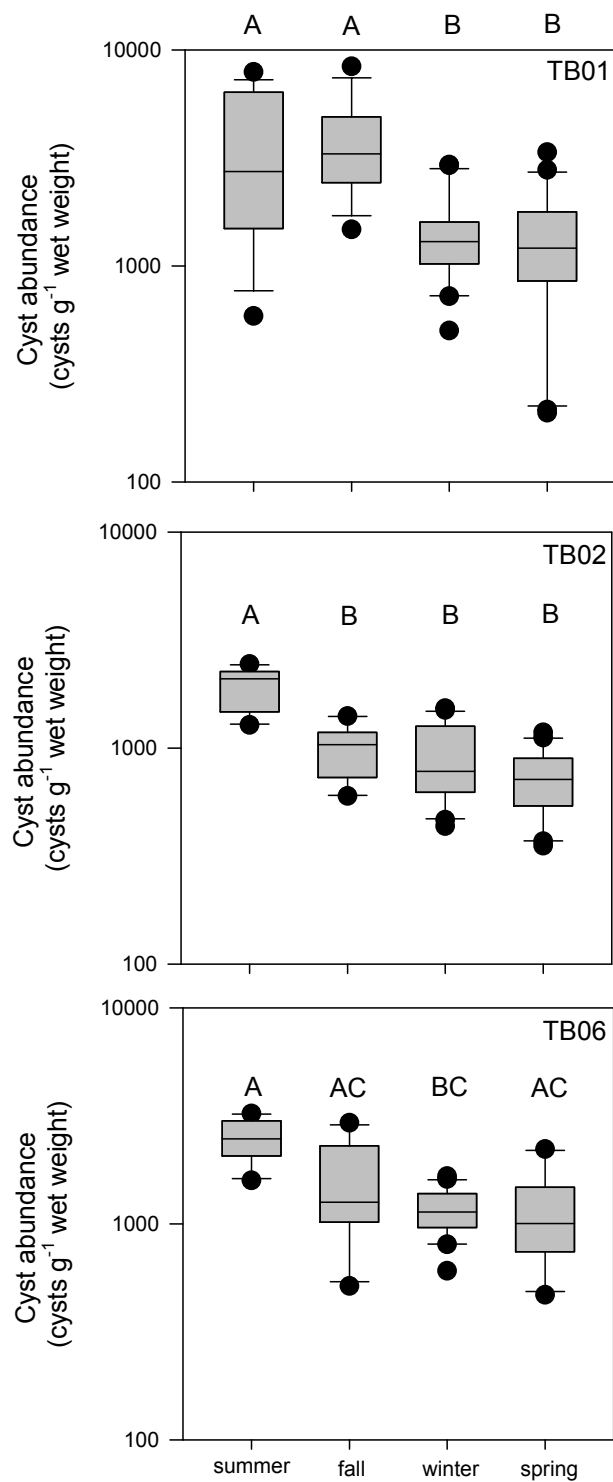


Figure 4. Cyst abundance distributions (boxes indicate 25% and 75% quartiles, line represents median) by season in the upper five centimeters of sediment for TB01 (upper panel), TB02 (middle panel), and TB06 (lower panel). Similar letters among seasons indicate no significant difference.

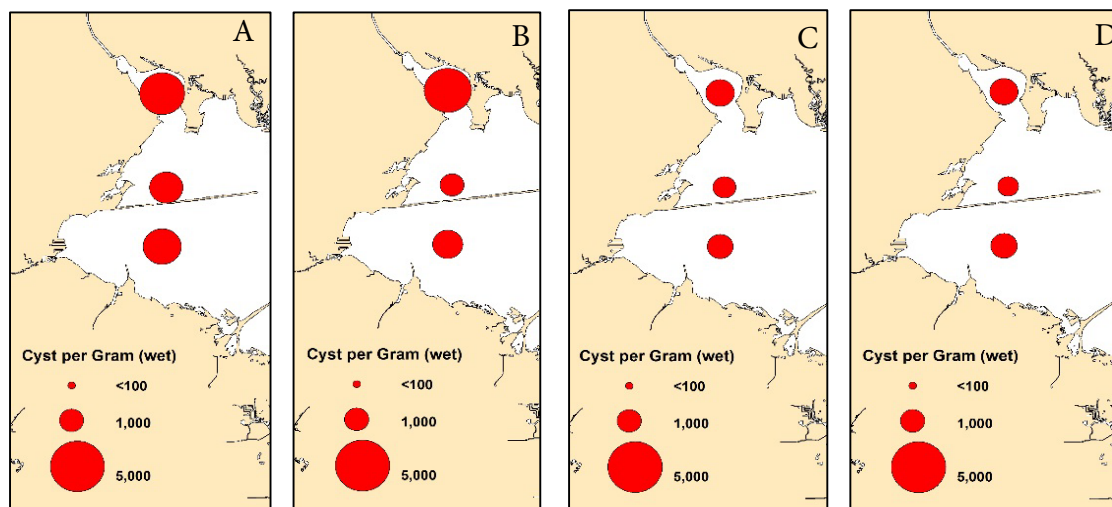


Figure 5. Cyst abundance at our three sites for (A) summer 2015, (B) fall 2015, (C) winter 2016, and (D) spring 2016.

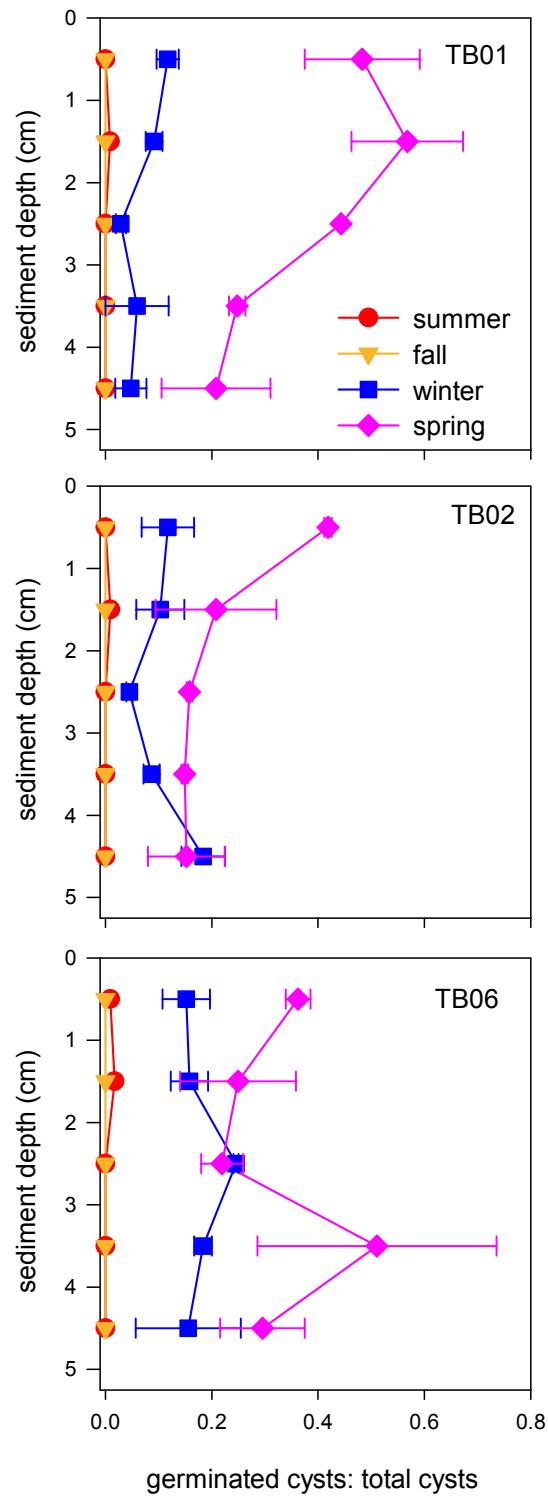


Figure 6. Vertical profiles of the fraction of cysts that germinated (mean \pm standard error of section replicates) in the upper five centimeters of sediment for TB01 (upper panel), TB02 (middle panel), and TB06 (lower panel).

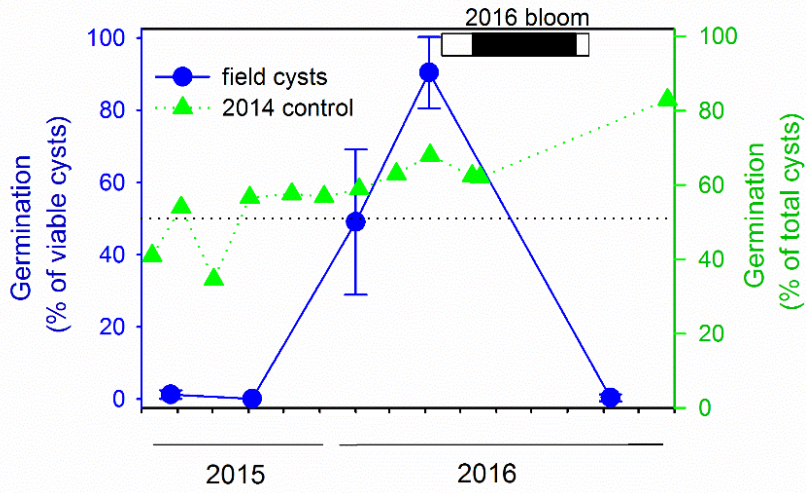


Figure 7. Time course of the fraction of viable field-collected cysts (blue, % mean and standard error of station replicates) and of non-dormant stored cysts (green) that germinated when isolated from sediment and incubated. The 2016 bloom period is highlighted by the black bar.

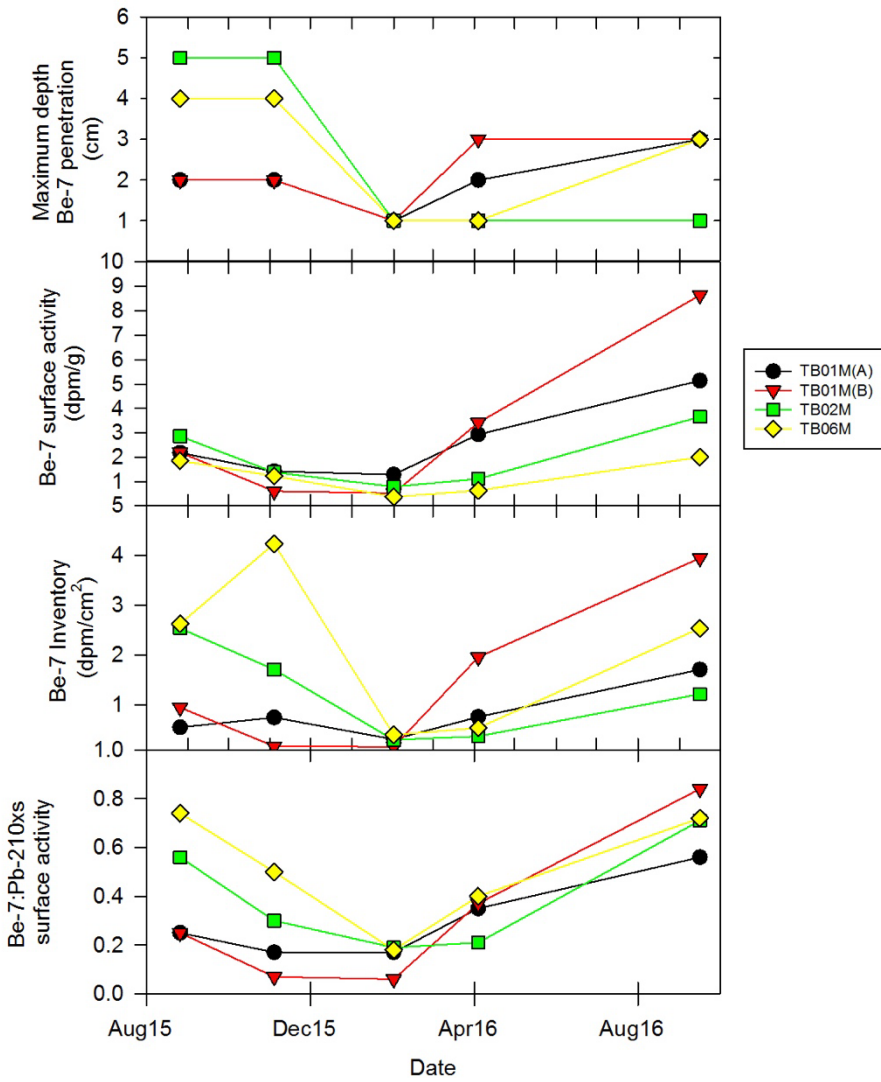


Figure 8. Time-series plot for each of the sites (color coded in each figure) of ⁷Be penetration vertical downward in the sediment (first panel), the activity of ⁷Be measured in the 0-1 cm sample of each core (second panel), the depth integrated inventory (third panel), and the activity ratio of ⁷Be and ²¹⁰Pb measured during this study.

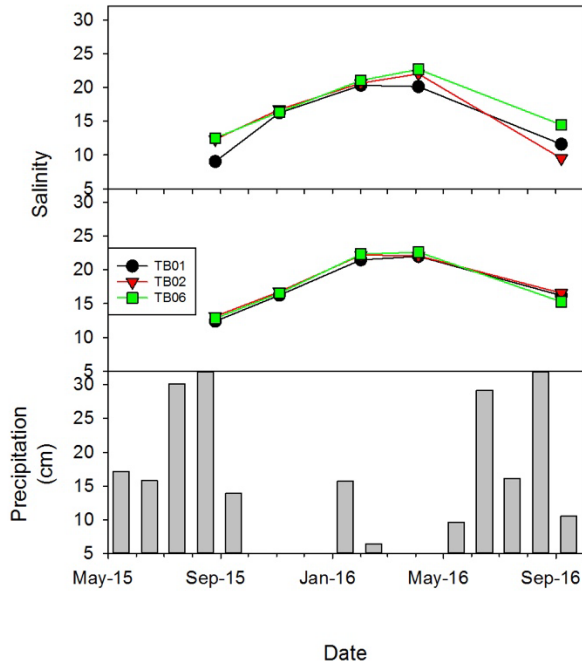


Figure 9. Plot of surface water (top) and bottom water (middle) salinity measured during the five different sampling trips. The trend in salinity is a reflection of freshwater inputs inevitably due to the monsoonal climate present in west-central Florida (precipitation, bottom panel).

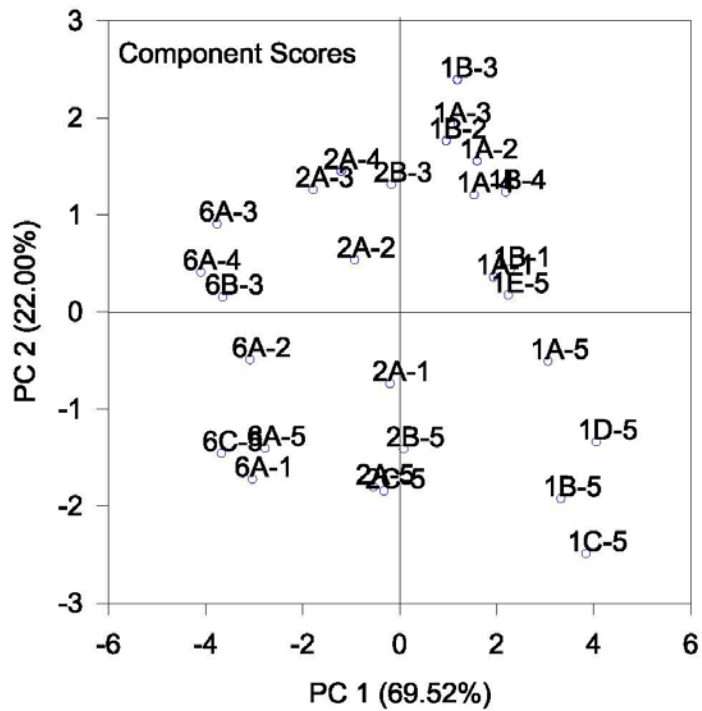
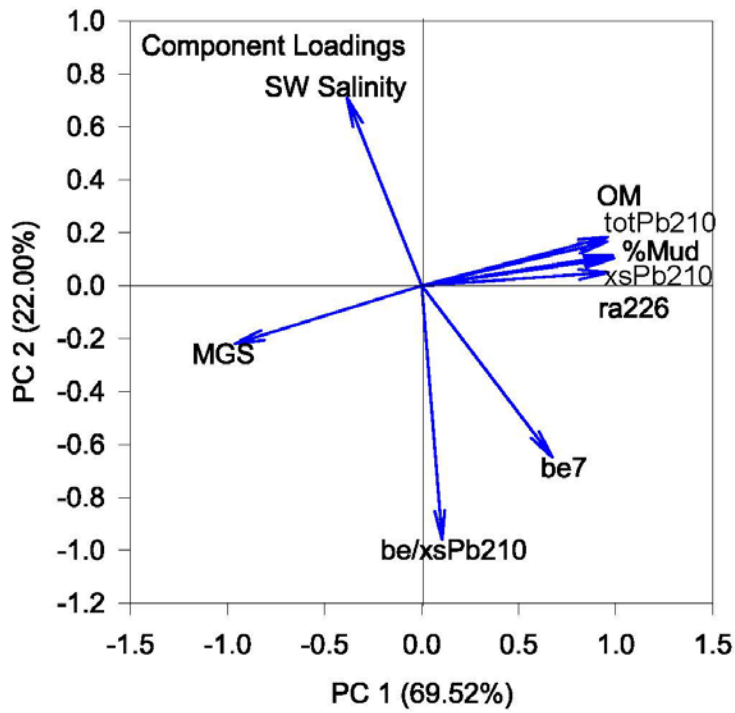


Figure 10. Component loadings (top panel) vector diagram showing the relationship among salinity as well as physical and radiochemical properties of surface sediments for the entire study (space and time). The result sample scores show the strong “upstream”-to-“downstream” character of the entire study are.

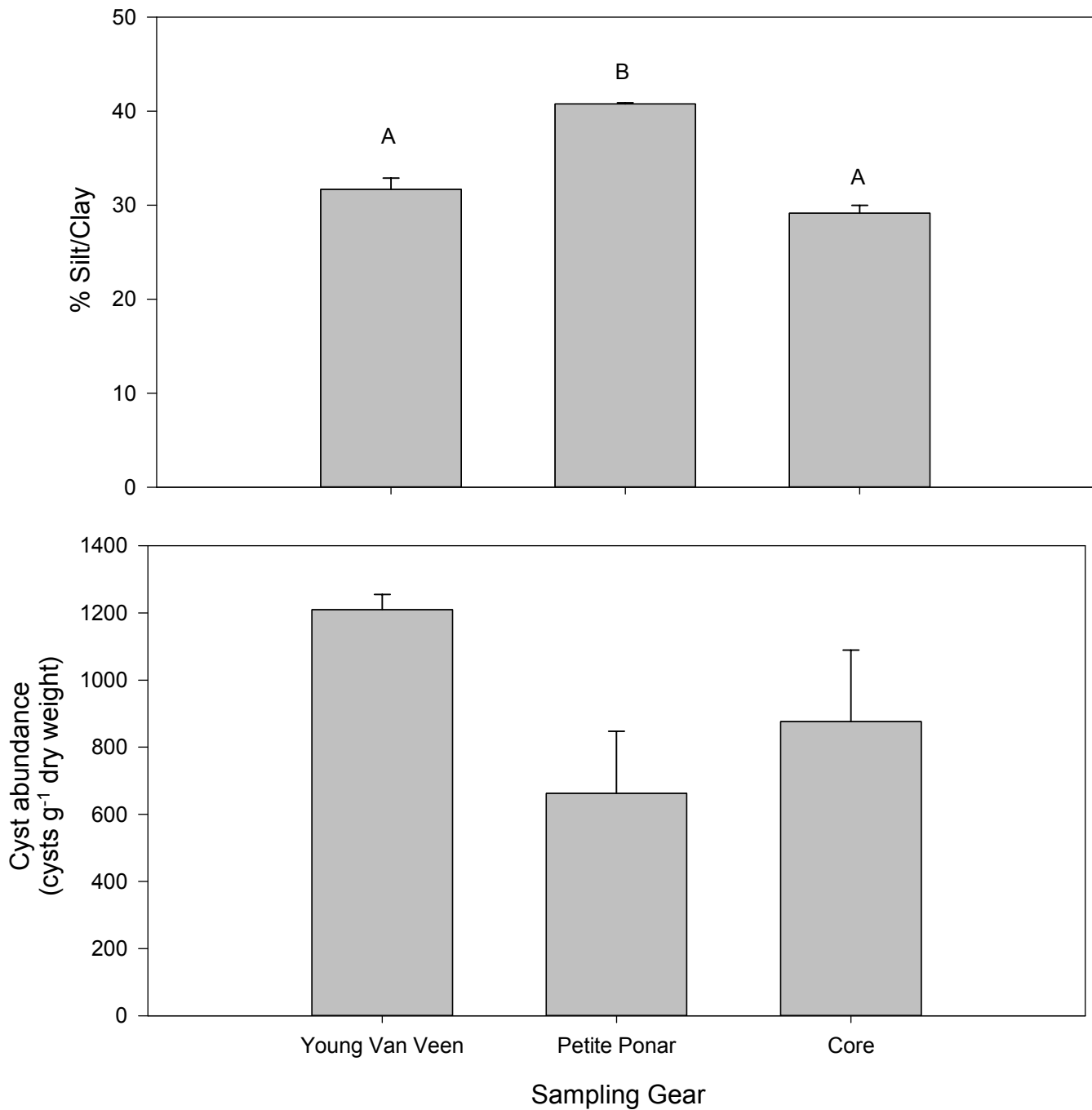


Figure 11. Mean and standard error of % silt/clay (top panel) and cyst abundance (bottom panel) among different sampling gear. Different letters in top panel indicate significant differences.

APPENDIX

Sediment Profiles

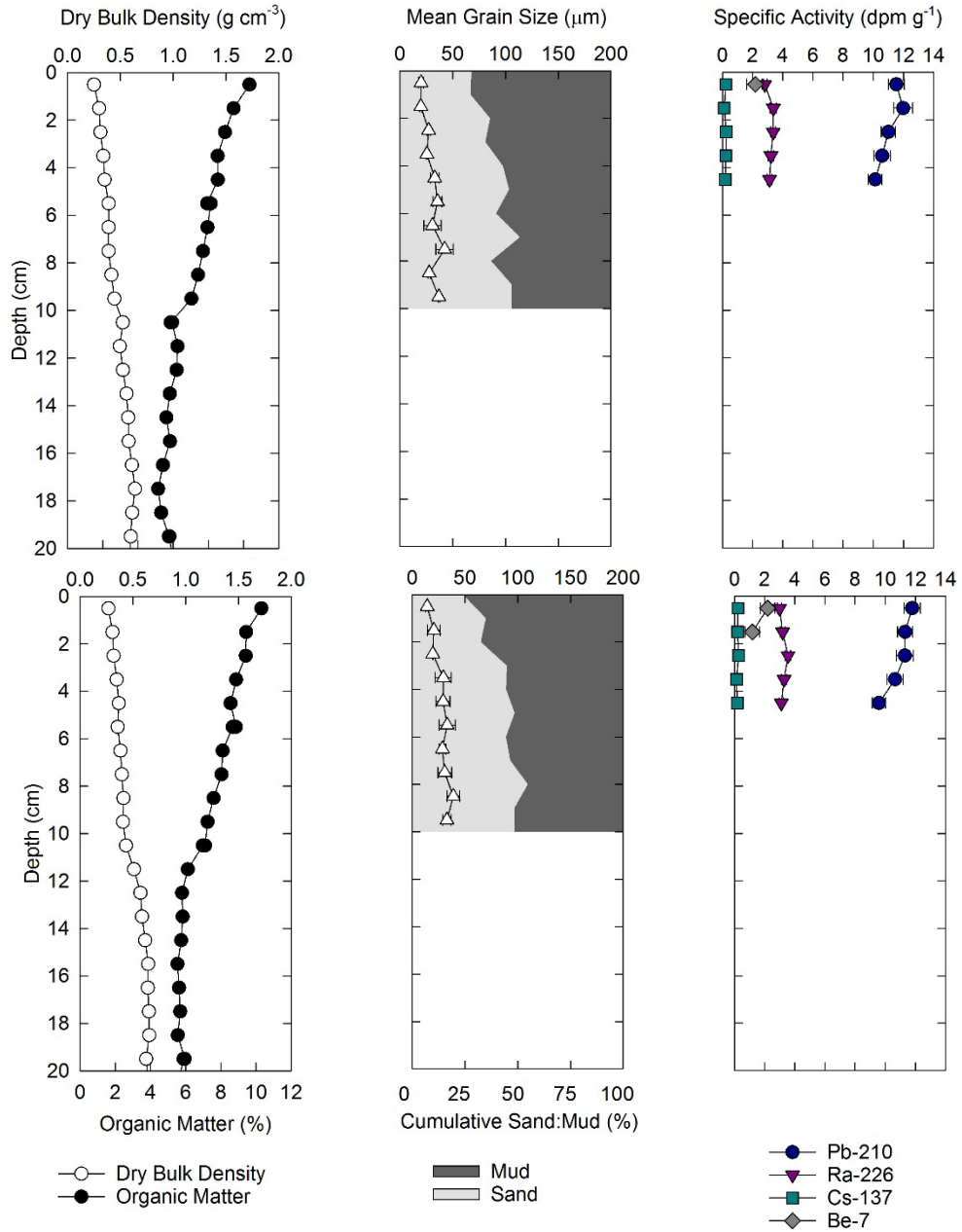


Figure A1. TB01-A (upper panels) and TB01-B (lower panels) sediment profiles for summer 2015.

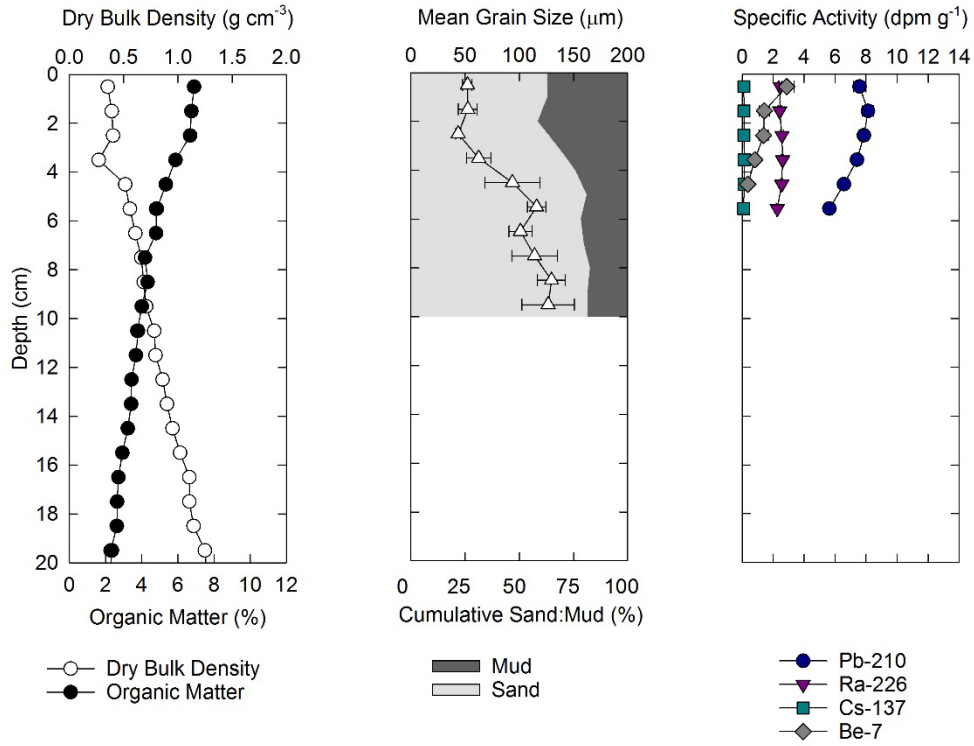


Figure A2. TB02 sediment profiles for summer 2015.

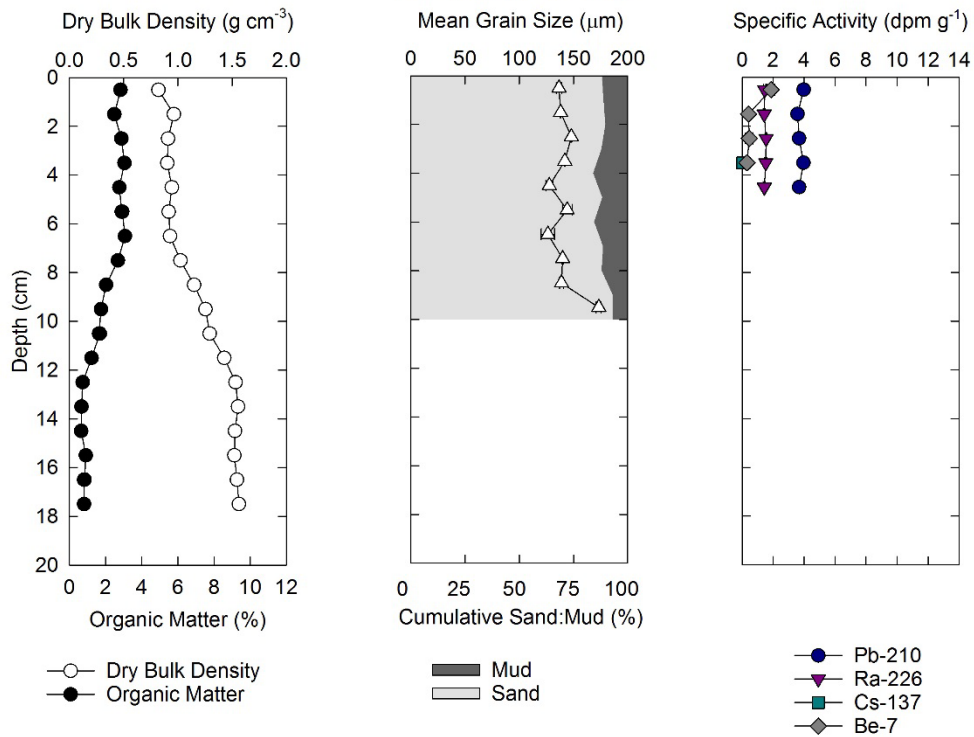


Figure A3. TB06 sediment profiles for summer 2015.

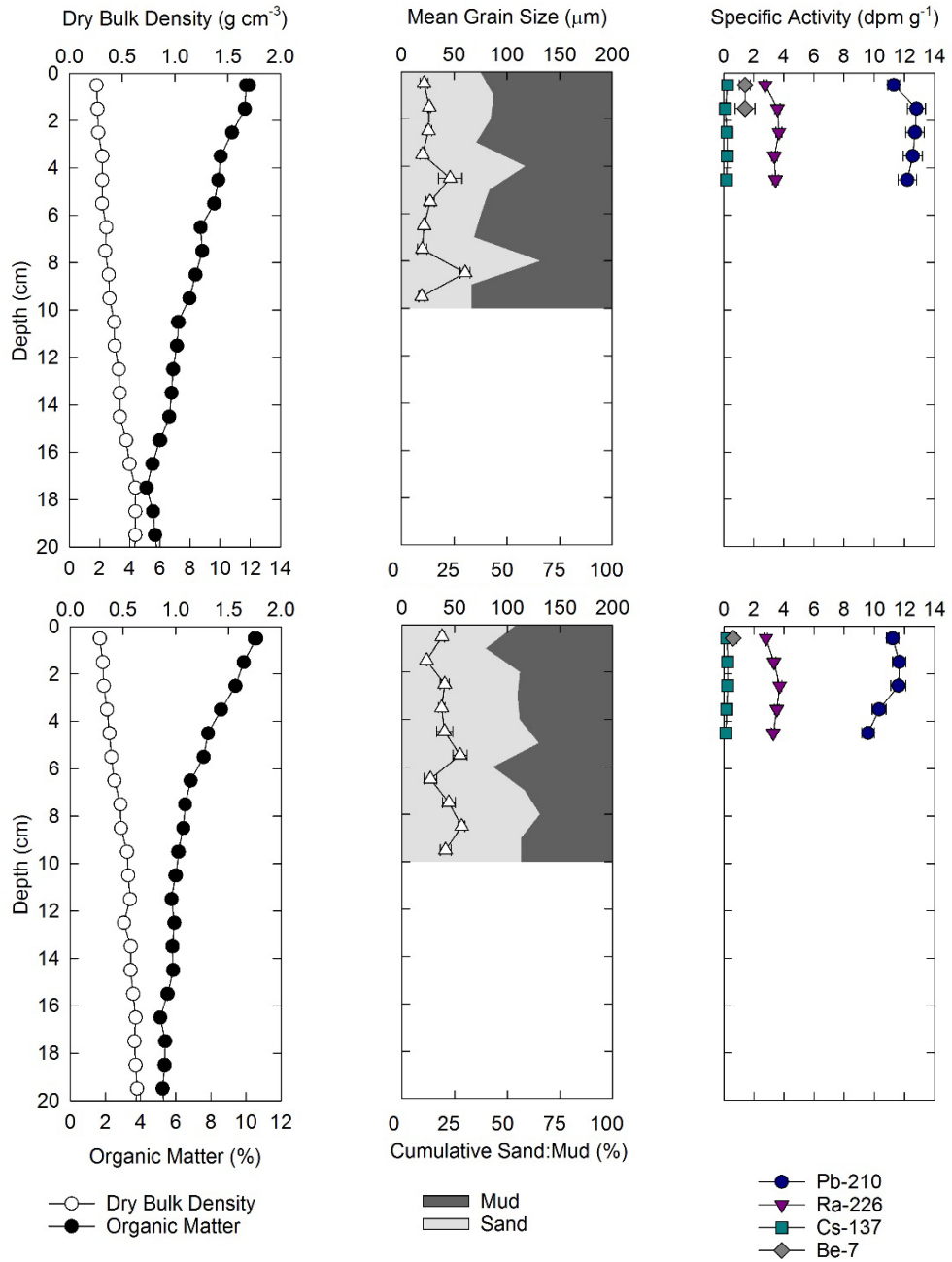


Figure A4. TB01-A (upper panels) and TB01-B (lower panels) sediment profiles for fall 2015.

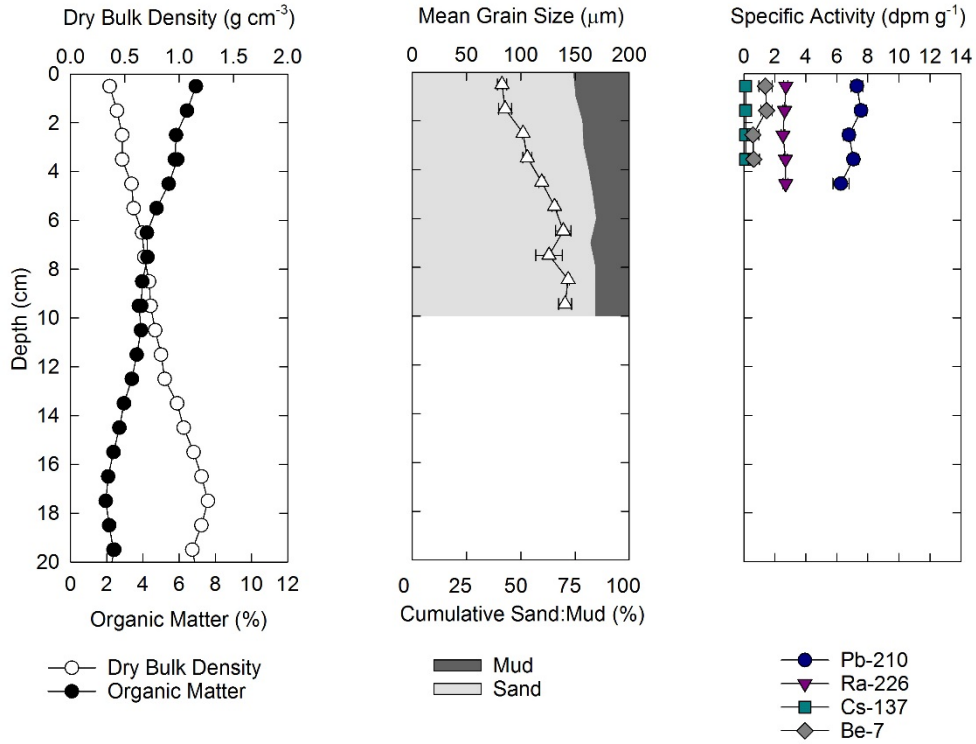


Figure A5. TB02 sediment profiles for fall 2015.

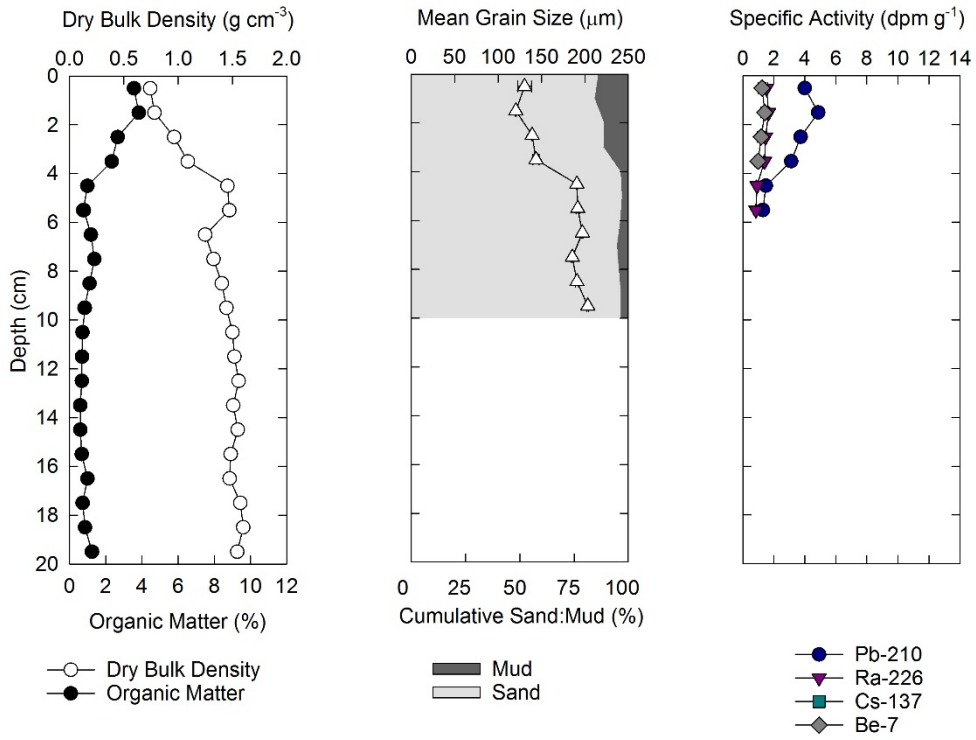


Figure A6. TB06 sediment profiles for fall 2015.

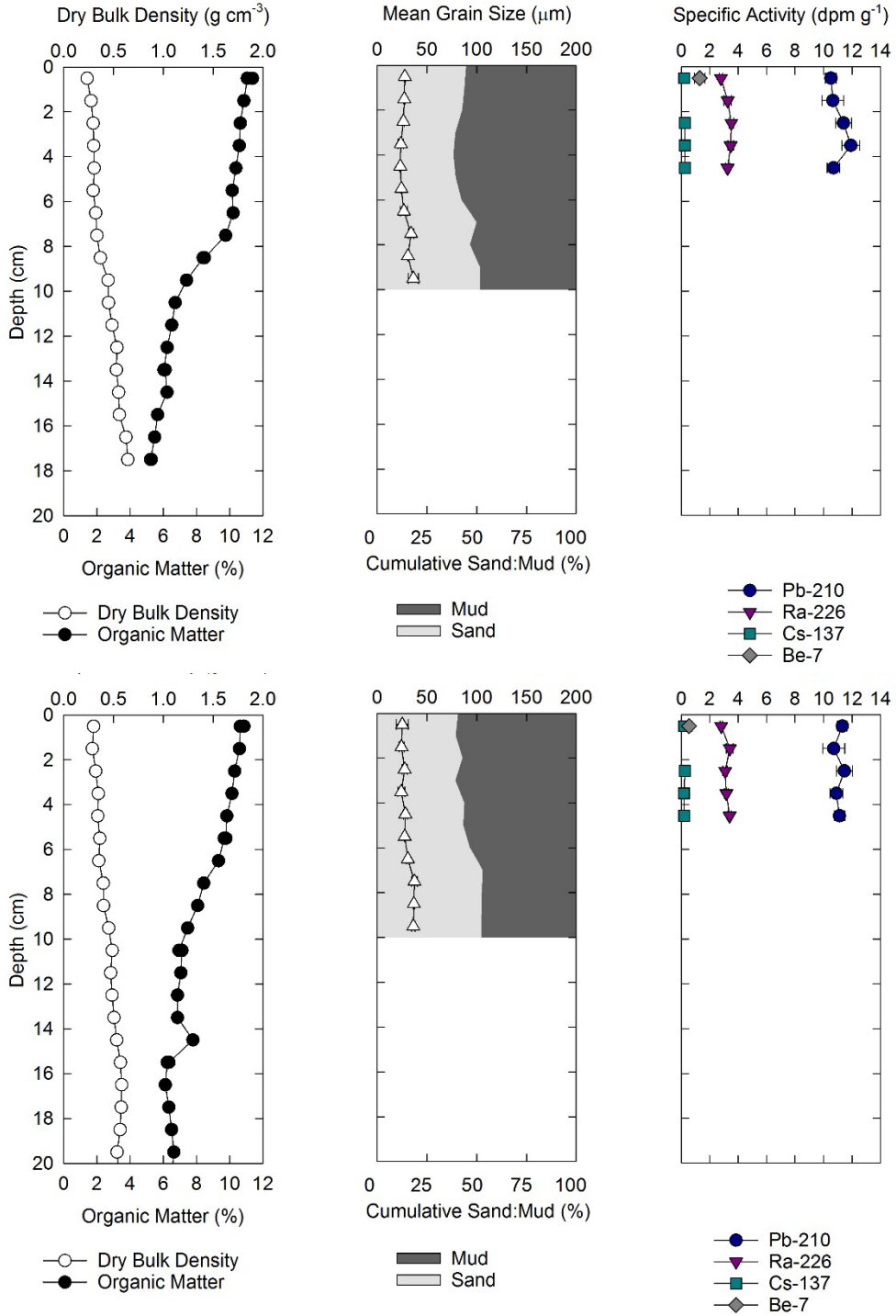


Figure A7. TB01-A (upper panels) and TB01-B (lower panels) sediment profiles for winter 2016.

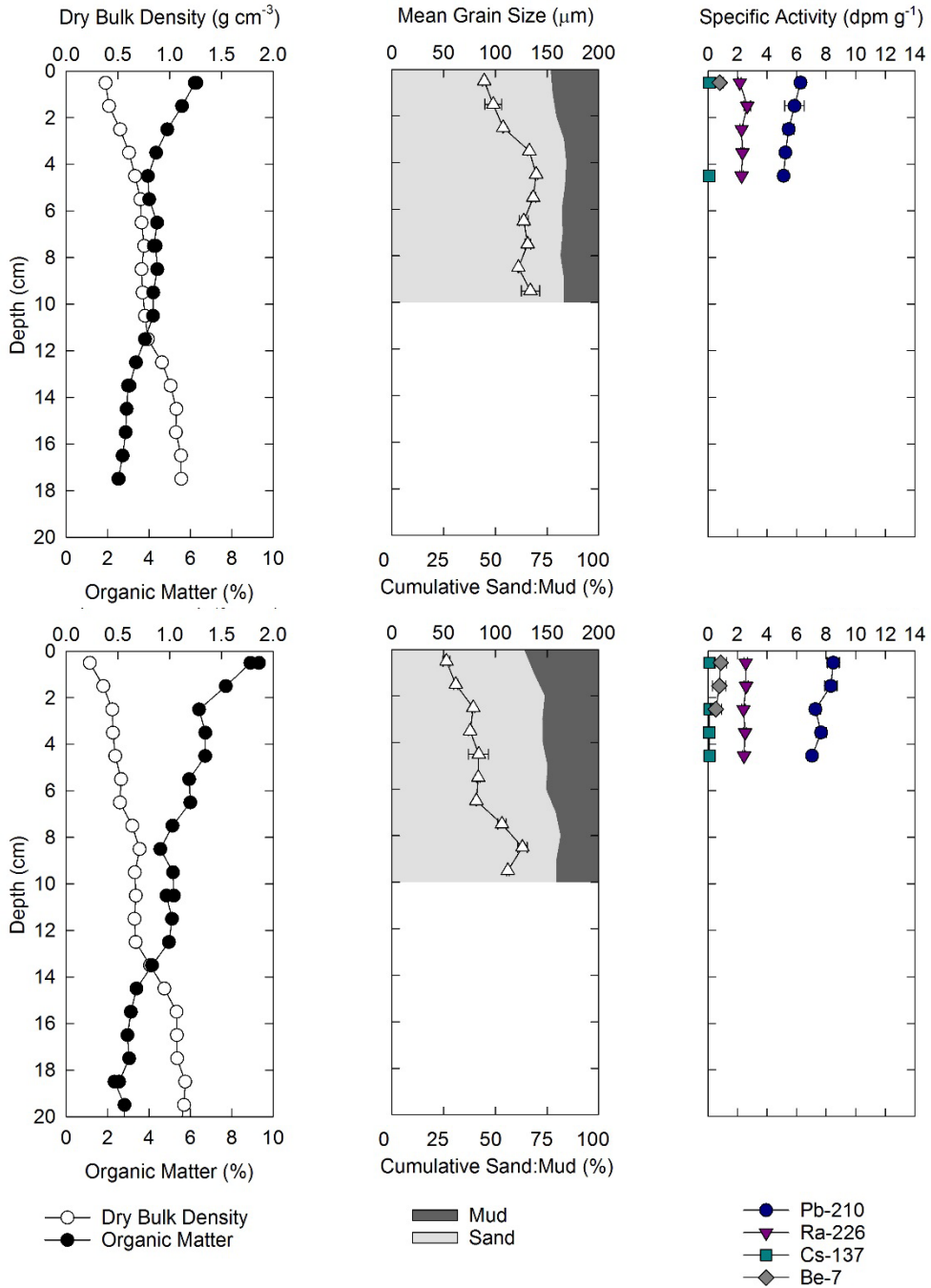


Figure A8. TB02-A (upper panels) and TB02-B (lower panels) sediment profiles for winter 2016.

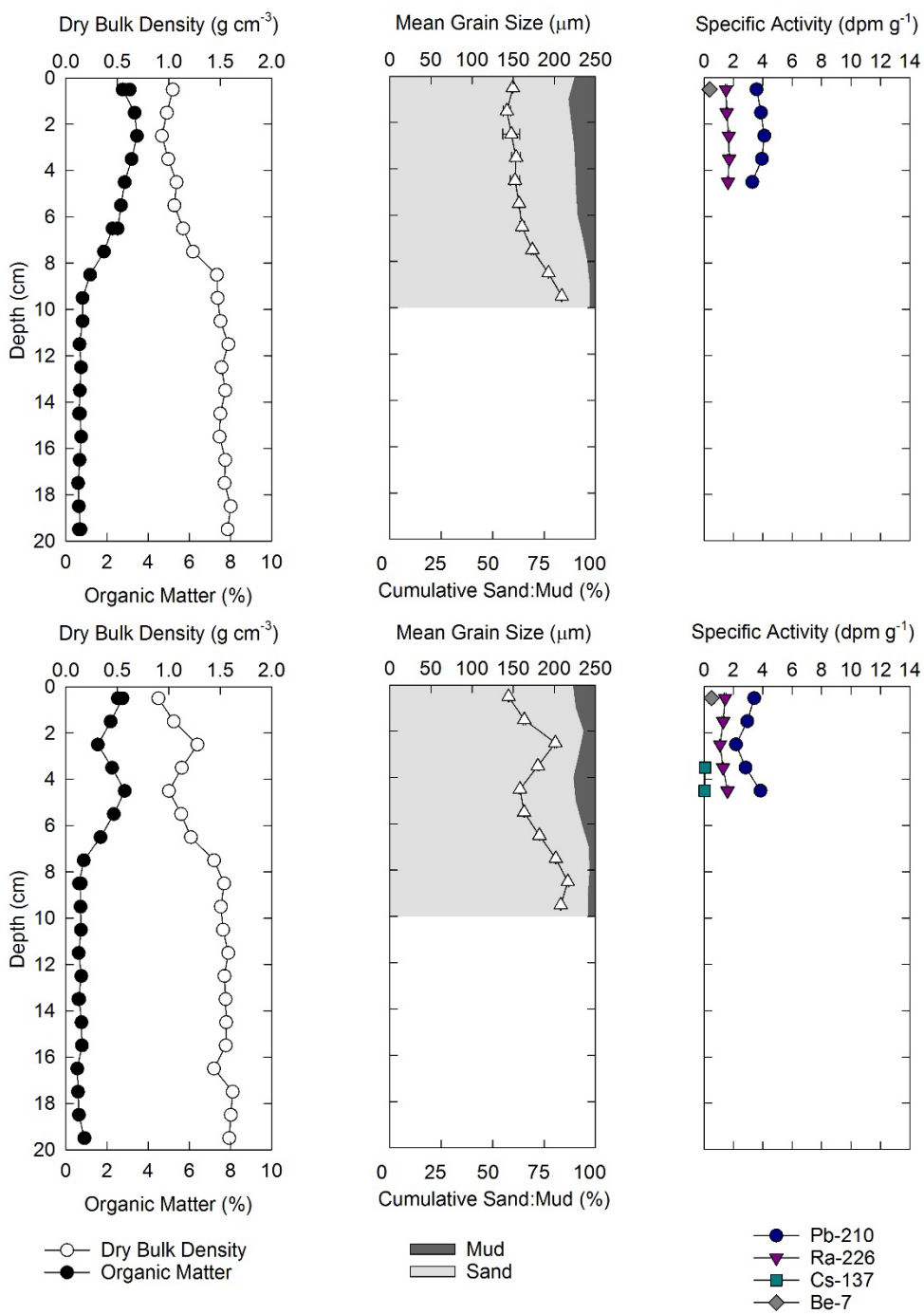


Figure A9. TB06-A (upper panels) and TB06-B (lower panels) sediment profiles for winter 2016.

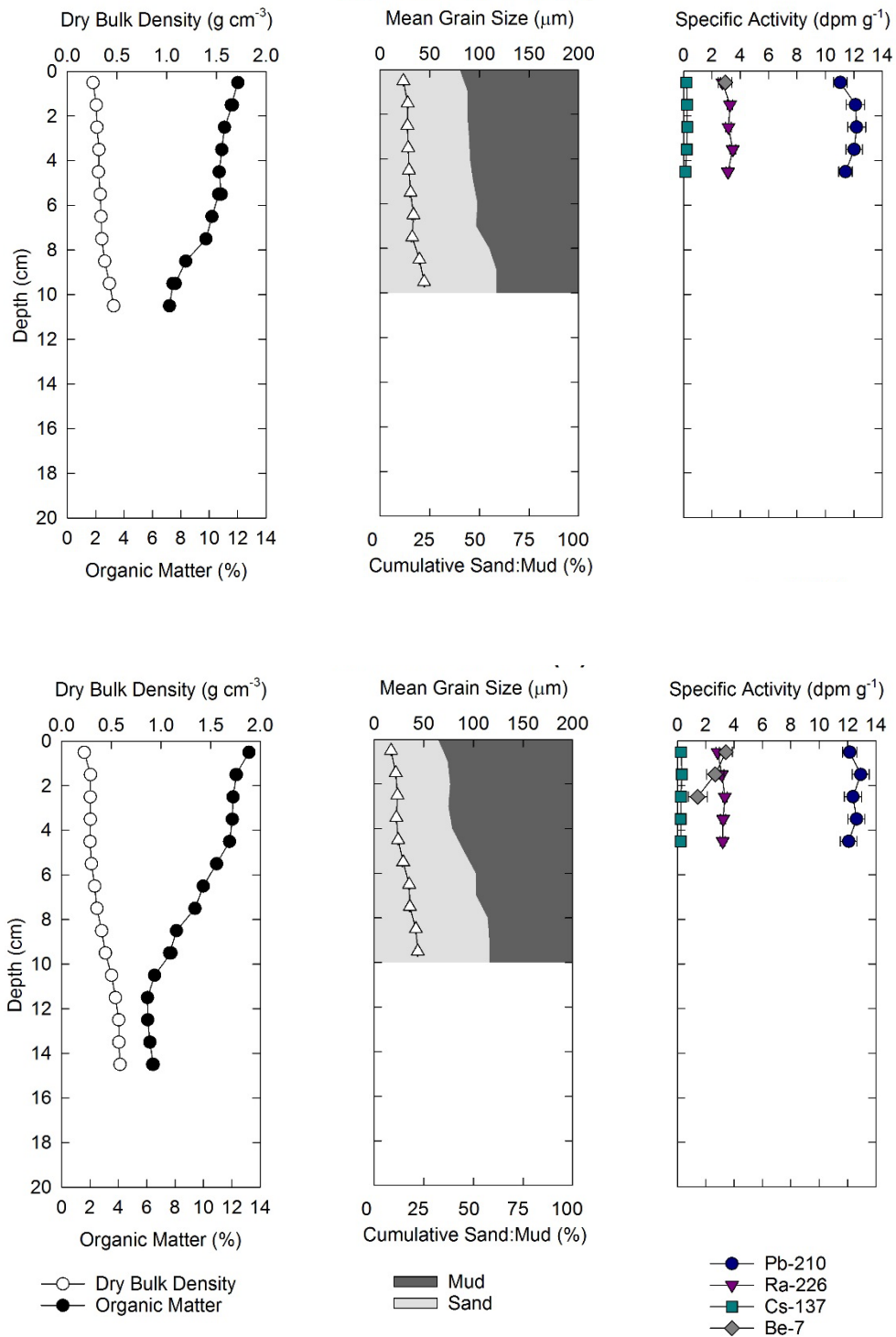


Figure A10. TB01-A (upper panels) and TB01-B (lower panels) sediment profiles for spring 2016.

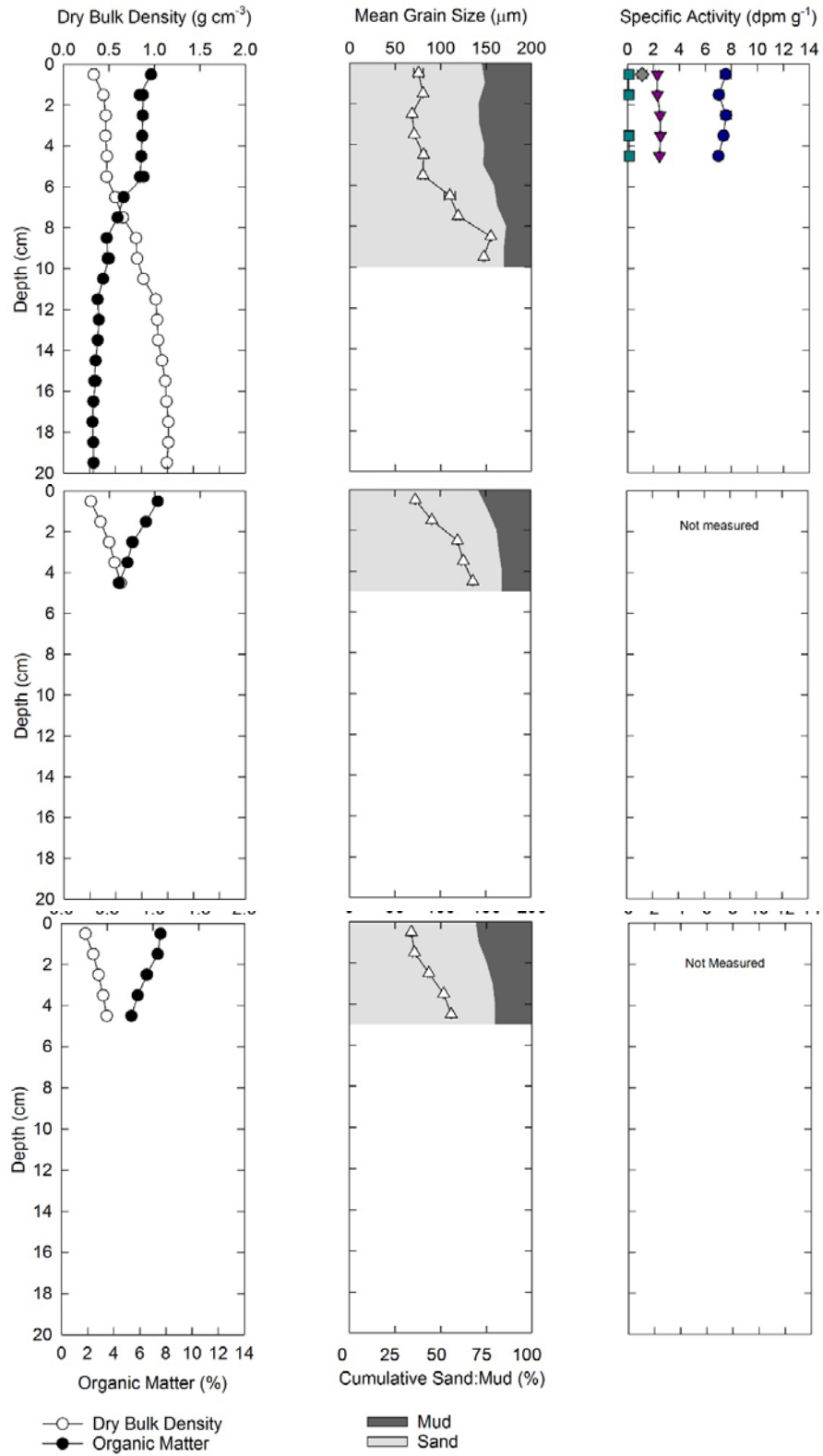


Figure A11. TB02-A (upper), TB02-B (middle, and TB02-C (lower) sediment profiles for spring 2016.

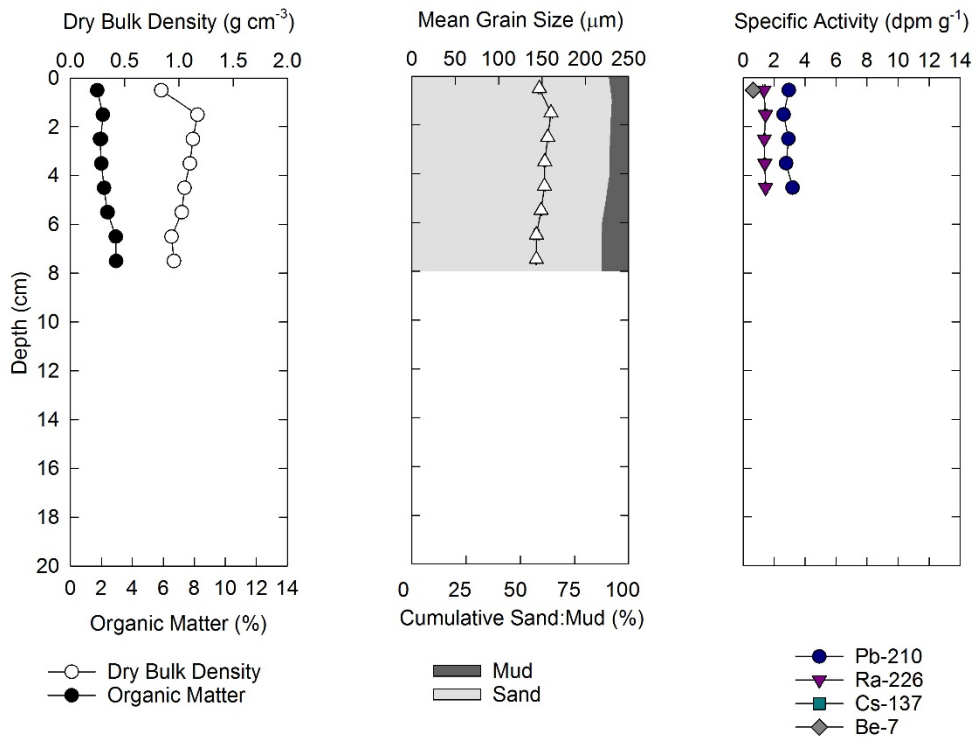


Figure A12. TB06 sediment profiles for spring 2016.

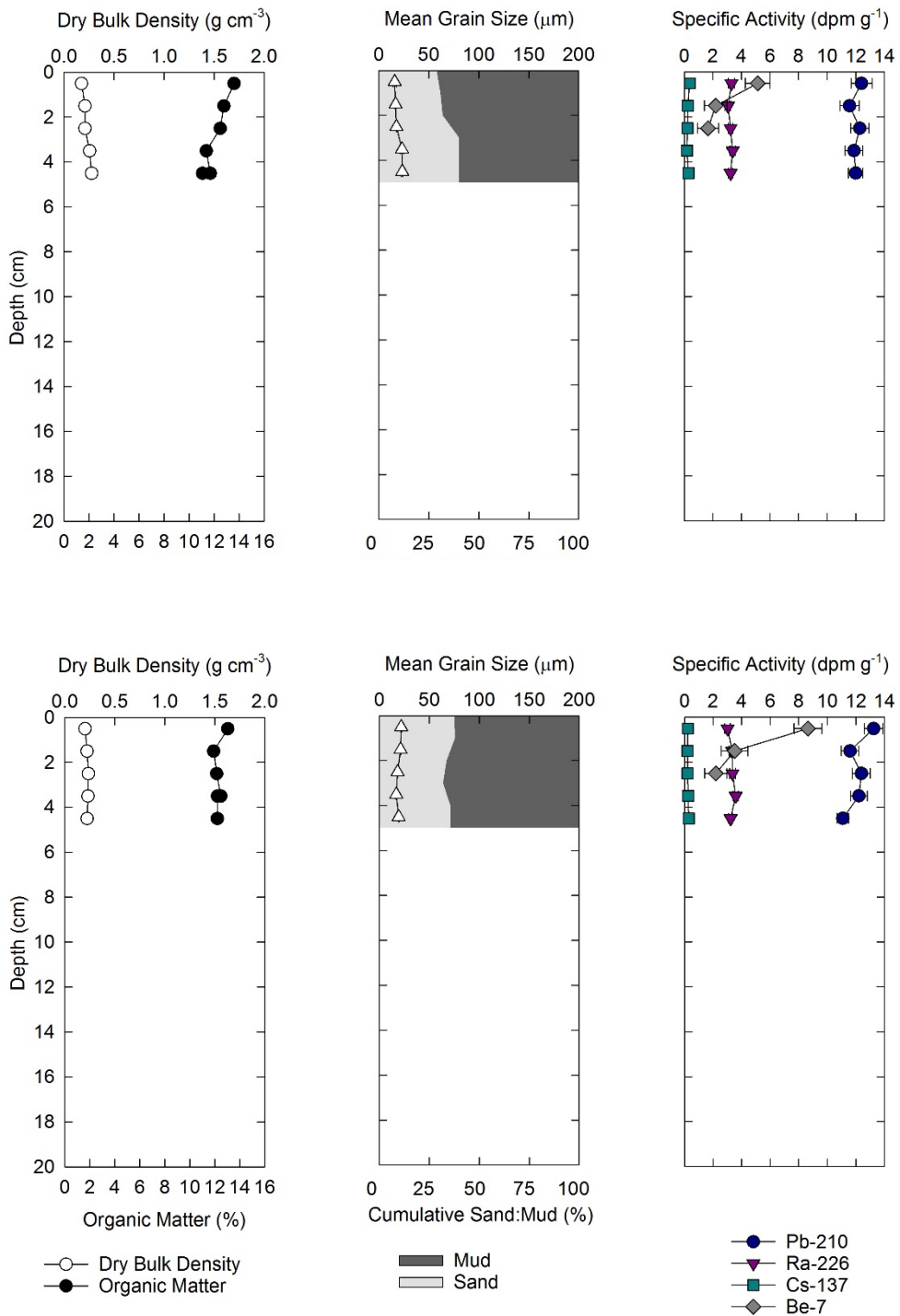


Figure A13. TB01-A (upper panels) and TB01-B (lower panels) sediment profiles for summer 2016.

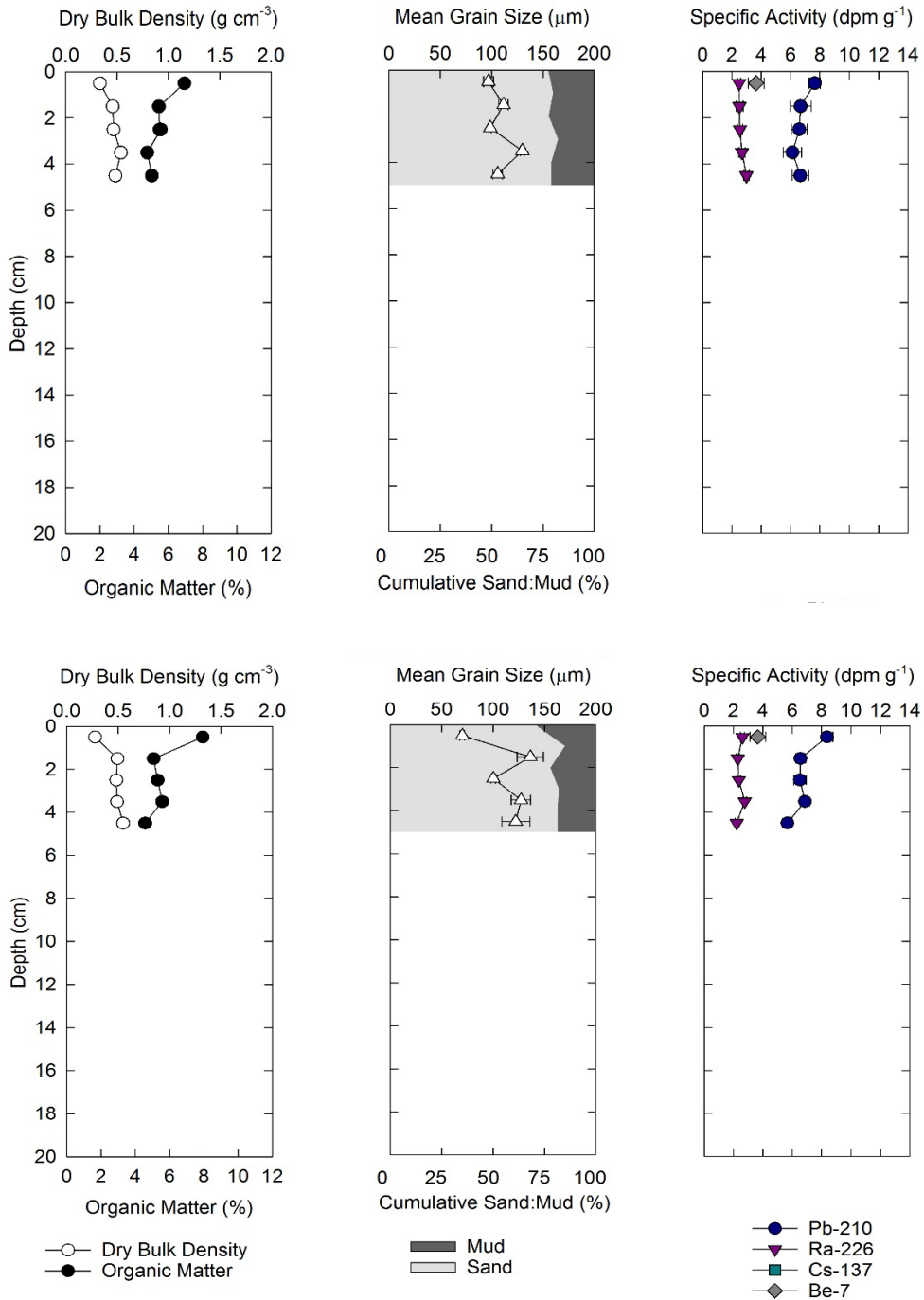


Figure A14. TB02-A (upper panels) and TB02-B (lower panels) sediment profiles for summer 2016.

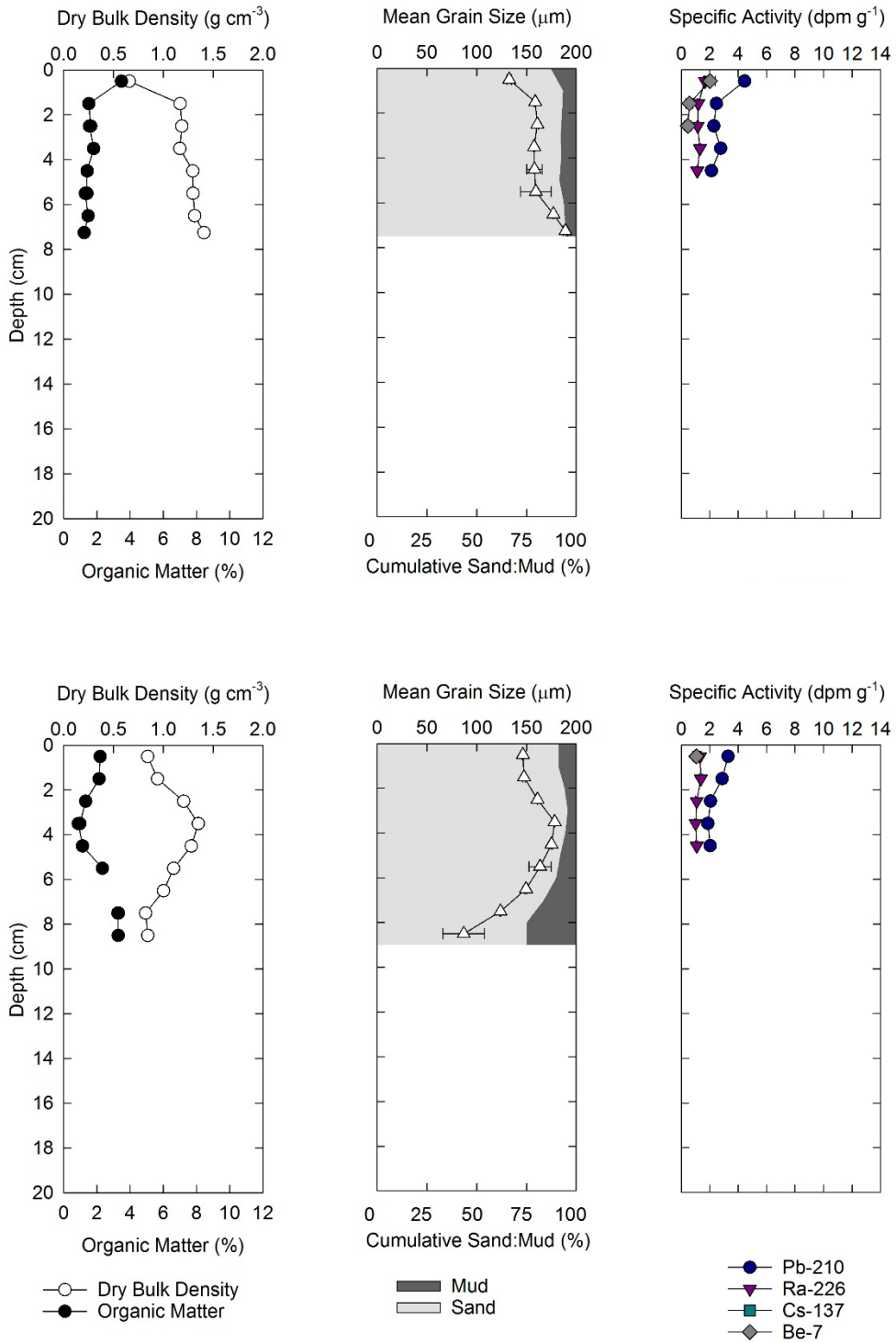


Figure A15. TB06-A (upper panels) and TB06-B (lower panels) sediment profiles for summer 2016.